AGU PUBLICATIONS

JGR

Journal of Geophysical Research: Biogeosciences

RESEARCH ARTICLE
10.1002/2016JG003467

Key Points:
- Linking stomatal response to stem water potential improves transpiration prediction
- FETCH2 simulates aboveground water storage, sap flux, and transpiration
- FETCH2 shows differences in isohydric/anisohydric behavior on stomatal conductance

Supporting Information:
- Supporting Information S1
- Data Set S1
- Data Set S2
- Data Set S3

Correspondence to:
G. Mirfenderesgi,
mirfenderesgi.1@osu.edu

Citation:
Mirfenderesgi, G., G. Bohrer, A. M. Matheny, S. Fatichi, R. P. de M. Frasson, and K. V. R. Schäfer (2016), Tree level hydrodynamic approach for resolving aboveground water storage and stomatal conductance and modeling the effects of tree hydraulic strategy, *J. Geophys. Res. Biogeosci.*, *121*, doi:10.1002/2016JG003467.

Received 27 APR 2016
Accepted 17 JUN 2016
Accepted article online 21 JUN 2016

Tree level hydrodynamic approach for resolving aboveground water storage and stomatal conductance and modeling the effects of tree hydraulic strategy

Golnazalsadat Mirfenderesgi[1], Gil Bohrer[1], Ashley M. Matheny[1], Simone Fatichi[2], Renato Prata de Moraes Frasson[3], and Karina V. R. Schäfer[4]

[1]Department of Civil, Environmental, and Geodetic Engineering, Ohio State University, Columbus, Ohio, USA, [2]Institute of Environmental Engineering, ETH Zurich, Zurich, Switzerland, [3]Byrd Polar and Climate Research Center, Ohio State University, Columbus, Ohio, USA, [4]Department of Biological Sciences, Rutgers University, Newark, New Jersey, USA

Abstract The finite difference ecosystem-scale tree crown hydrodynamics model version 2 (FETCH2) is a tree-scale hydrodynamic model of transpiration. The FETCH2 model employs a finite difference numerical methodology and a simplified single-beam conduit system to explicitly resolve xylem water potentials throughout the vertical extent of a tree. Empirical equations relate water potential within the stem to stomatal conductance of the leaves at each height throughout the crown. While highly simplified, this approach brings additional realism to the simulation of transpiration by linking stomatal responses to stem water potential rather than directly to soil moisture, as is currently the case in the majority of land surface models. FETCH2 accounts for plant hydraulic traits, such as the degree of anisohydric/isohydric response of stomata, maximal xylem conductivity, vertical distribution of leaf area, and maximal and minimal xylem water content. We used FETCH2 along with sap flow and eddy covariance data sets collected from a mixed plot of two genera (oak/pine) in Silas Little Experimental Forest, NJ, USA, to conduct an analysis of the intergeneric variation of hydraulic strategies and their effects on diurnal and seasonal transpiration dynamics. We define these strategies through the parameters that describe the genus level transpiration and xylem conductivity responses to changes in stem water potential. Our evaluation revealed that FETCH2 considerably improved the simulation of ecosystem transpiration and latent heat flux in comparison to more conventional models. A virtual experiment showed that the model was able to capture the effect of hydraulic strategies such as isohydric/anisohydric behavior on stomatal conductance under different soil-water availability conditions.

1. Introduction

Transpiration is controlled by the atmospheric demand for moisture and limited by stomatal conductance that is regulated to a certain extent by the plant water status and thus water availability. Most current land surface and hydrologic models impose water availability limitations on stomatal conductance using simple linear Feddes-type [*Feddes et al.*, 2001, 1976] or sigmoidal [*Jarvis*, 1976] empirical relationships between stomatal conductance or photosynthetic capacity and soil moisture. These parameterizations link leaf stomatal conductance directly and instantaneously to soil moisture and do not incorporate mechanistic representation of the internal water storage and flow through the vegetation, xylem hydraulic properties, or stem and canopy structure. Models that do not represent the plant water storage-mediated regulation of stomatal conductance are potentially too sensitive to soil water potential or atmospheric vapor pressure deficit (VPD) variations and may misrepresent the intradaily dynamics of transpiration [*Matheny et al.*, 2014b].

Plant water storage and its diurnal dynamics provide one of the mechanisms that influence the magnitude of the diurnal hysteretic pattern of transpiration. The hysteretic pattern is formed when, for the same atmospheric demand for water vapor and soil moisture conditions, plants transpire more before noon than during the afternoon [*Matheny et al.*, 2014b; *Novick et al.*, 2014; *O'Brien et al.*, 2004; *Unsworth et al.*, 2004; *Verbeeck et al.*, 2007a, 2007b; *Zhang et al.*, 2014]. Regulation of stomatal conductance due to leaf level water stress is known to affect transpiration when the soil is dry or when VPD is high [*Brodribb and Holbrook*, 2004; *Davis et al.*, 2002; *McCulloh and Sperry*, 2005; *Monteith*, 1995; *Turner et al.*, 1984]. Nonetheless, it can also

impact stomatal apertures under conditions of adequate soil moisture and lower evaporative demand, if depletion of water in the leaves occurs at a faster rate than recharge of the stem xylem [*Brodribb and Holbrook*, 2004; *Ewers et al*., 2007a, 2007b; *McCulloh et al*., 2012; *Sperry et al*., 2002]. As such, photosynthesis and the coupled water and energy cycles substantially deviate from the predictions of models that employ a direct link to soil moisture, which, in turn, leads to biases in diurnal dynamics of simulated transpiration [*Matheny et al*., 2014a].

The physiological mechanisms for avoidance of hydraulic failure modify stomatal opening and control water loss at the cost of reduced carbon assimilation [*Cowan and Farquhar*, 1977; *Katul et al*., 2003; *McDowell et al*., 2008, 2013; *Meinzer et al*., 2013]. The degree and intensity of this hydraulic regulation vary among species and with the size and structure of the plant [*Buckley*, 2005; *Maherali et al*., 2006, 2004; *Matheny et al*., 2014a; *Meinzer et al*., 2003; *Meinzer and McCulloh*, 2013; *Meinzer et al*., 2014; *Pittermann et al*., 2005; *Tardieu and Davies*, 1993; *Tardieu and Simonneau*, 1998; *Thomsen et al*., 2013; *Whitehead*, 1998]. Plants regulate their leaf water status by modifying stomatal conductance using a range of strategies: from isohydric—relatively constant leaf water potential actively maintained by stomatal regulation—to anisohydric—minimal stomatal regulation resulting in varying leaf water potential typically driven by the balance of water supply to the leaf and atmospheric demand. Isohydric versus anisohydric regulation of leaf water status affects transpiration and carbon assimilation under regular conditions and in response to disturbance and drought [*Anderegg et al*., 2012; *Franks et al*., 2007; *Gentine et al*., 2015; *Güneralp and Gertner*, 2007; *Kolb and McCormick*, 1993; *McDowell et al*., 2008; *Meinzer et al*., 2014; *Ogle et al*., 2000; *Roman et al*., 2015; *Tardieu and Simonneau*, 1998].

We hypothesize that because of their more dynamic stomatal control, isohydric trees typically close their stomata earlier in days when low soil moisture and high atmospheric demand reduce xylem water pressure faster than during days when soil moisture is nonlimiting. Anisohydric trees show less severe daily fluctuations in stomatal conductance, but stronger fluctuations in xylem water potential and thus the amount of aboveground water storage [*Matheny et al*., 2015; *Meinzer et al*., 2014]. These differences between trees will affect the overall plot level transpiration, and particularly the intradaily dynamics of transpiration, especially when soil moisture is intermediate.

Mechanistically resolving xylem water potential allows the quantification of differences in transpiration and water stress between isohydric and anisohydric trees in the same site and soil moisture conditions, and defines the parameters that describe the traits that control these aspects of plant hydraulic response. We will demonstrate that by mechanistically resolving the aboveground xylem water potentials, stem water storage, and leaf hydraulic strategies of trees that we will be able to model the distinct behaviors of species throughout the isohydric-anisohydric trait continuum in response to drying soil conditions. Furthermore, tree level results can be statistically scaled to the plot level and achieve increased accuracy in the simulation of ecosystem-scale transpiration fluxes. We used a novel tree hydrodynamic model, and observations of tree level sap flow and plot level eddy flux from an oak/pine forest in the New Jersey Pine Barrens, a nutrient-poor and water-limited environment [*Dighton et al*., 2004; *Pan et al*., 2006; *Renninger et al*., 2014; *Schäfer et al*., 2010], to test our hypothesis.

2. Materials and Methods

2.1. Model Description

We developed the finite difference ecosystem-scale tree crown hydrodynamics model version 2 (FETCH2). FETCH2 solves Richards' equation to simulate xylem water pressure and consequent stomatal conductance of a tree crown. The Richards' equation analogy for xylem water flow established by *Sperry et al*. [1998] has been broadly applied [*Chuang et al*., 2006; *Früh and Kurth*, 1999; *Kumagai*, 2001; *Mackay et al*., 2015; *Verma et al*., 2014]. Additionally, some advanced models include a capacitance term to account for canopy water storage using an analogous electric circuit formulation [e.g., *Boersma et al*., 1991; *Bonan et al*., 2014; *Cowan*, 1972; *Lee*, 1992; *Sheriff*, 1973; *Sperry et al*., 1998; *Steppe et al*., 2006; *Tyree et al*., 1994; *Van den Honert*, 1948] or by water mass budget through the stem volume [*Gentine et al*., 2015]. However, the hydrodynamics of water flow through xylem is more complex than the dynamics described by electric-equivalence capacitor models [*Chuang et al*., 2006]. Therefore, a few models that resolve stem water potential using a mechanistic representation of porous medium flow through the stem have been introduced [*Bohrer et al*., 2005; *Janott et al*., 2011; *Nikinmaa et al*., 2014]. Nevertheless, such models are computationally intensive and can currently

Table 1. List of All Variables Used in FETCH2 Formulation

Parameter	Description	Units	Values
A_{Crown}	Genus-based mean crown area	m^2	
$A_{Crown,tot}$	Genus-based total crown area	m^2	
A_p	Total plot area	m^2	
$A_{p,tot}$	Genus-based total sapwood area	m^2	
A_{Sap}	Genus-based mean sapwood area (Active xylem)	m^2	
$A_{Sap,tot}$	Genus-based total sapwood area (Active xylem)	m^2	
A_{Stem}	Cross-section area of the entire stem	m^2	
B	Empirical shape parameter	-	
C	Capacitance of the active xylem	$kg_{H2O}\, m^{-1} MPa^{-1}$	
c_1	Shape parameter-cavitation pressure	Pa	
c_2	Shape parameter for conductance	-	
c_3	Shape parameter for stomatal response	-	
DBH	Diameter at breast height	cm	
El_c	Tree (crown) level water-limited transpiration water sink	$kg\, s^{-1}$	
El_p	Plot level water-limited transpiration water sink	Wm^{-2}_{ground}	
$ENHL_c$	Tree (crown) level NHL transpiration forcing	$kg\, s^{-1}$	
$ENHL_p$	Plot level NHL transpiration forcing	Wm^{-2}_{ground}	
$EOBS_p$	Plot level observed transpiration	Wm^{-2}_{ground}	
$EOBS_c$	Crown level observed transpiration	$kg\, s^{-1}$	
E_{sim}	Simulated plot level transpiration	Wm^{-2}_{ground}	
G	Gravitational acceleration	ms^{-2}	9.807
g_b	Leaf boundary layer conductance	$mol\, m^{-2} s^{-1}$	
g_s	Stomatal conductance	$mol\, m^{-2} s^{-1}$	
J_c	Tree level sap flux	$kg\, s^{-1}$	
J_p	Plot level sap flux	Wm^{-2}_{ground}	
$JOBS_c$	Observed tree sap flux	$kg\, m^{-1}\, s^{-1}$	
$JOBS_p$	Plot level observed sap flux	$W\, m^{-2}_{ground}$	
K	Conductivity of the active xylem	$m^2\, s$	
k	Conductance of the active xylem	s	
k_{max}	Maximum xylem conductance	s	
LAI_{Crown}	Genus level total leaf area to the total crown area of trees	$m^2_{leaf}\, m^{-2}_{crown}$	
$LEOBS_p$	Plot level observed latent heat flux	$W\, m^{-2}_{ground}$	
m	Fitting parameter of stomatal conductance model	-	
M_c	Total mass of water in the xylem of the tree	$kg\, m^{-2}_{stem}$	
NO	Number of free parameters in the model	-	
P	Atmospheric pressure	kPa	
P_0	Standard sea level atmospheric pressure	kPa	101.3
PAR	Photosynthetic active radiation	$\mu mol\, m^{-2}\, s^{-1}$	
R	Ideal gas constant adjusted for water vapor	$mol\, m^{-3}$	4.446×10^7
RL	Probability of information loss in a model	-	
RWC	Xylem relative water content	-	
S_c	Total storage of the tree	kg	
S_p	Plot level total storage of the tree	kg	
SD	Sapwood depth	cm	
T	Time	s	
t_{max}	End of simulation time	s	
T_a	Air temperature	°C	
T_0	Temperature conversion from °C to °K	-	273
U	Wind speed	$m\, s^{-1}$	
V_{cmax25}	Maximum carboxylation capacity of Rubisco at 25 °C	$\mu mol\, m^{-2}_{leaf}\, s^{-1}$	
VPD	Vapor pressure deficit	kPa	
V_{ToT}	Total occupied volume of the active xylem (including water and wood)	$m^3_{sapwood}\, m^{-2}_{stem}$	
x	Ratio of horizontal to vertical projections of leaves assumed spherical	-	
X_E	Xylem elasticity module	Pa	10^9
z	Vertical height of the tree	m	
z_{bottom}	Height at the base of the tree	m	

Table 1. (continued)

Parameter	Description	Units	Values
z_{top}	Height of the topmost element of the tree (tree height)	m	
β_s	Soil water stress function	-	
Δz	Length of the vertical elements of the tree	m	
Δt	Time step	s	
θ_{Sat}	Water content of saturated sapwood	$kg_{water}\, m^{-3}_{sapwood}$	
λ	Latent heat of vaporization	$kJ\, kg^{-1}$	2240
ρ	Water density	$kg_{H2O}\, m^{-3}_{sapwood}$	1000
σ^2	Variance of the error term	-	
σ_{obs}	Standard deviation of the observed plot level transpiration	Wm^{-2}	
ϕ_{x50}	Shape parameter—xylem water potential at 50% relative water content (RWC)	Pa	
ϕ_{x88}	Shape parameter—xylem water potential at 88% relative water content (RWC)	Pa	
Φ	Stem water potential	Pa	
Φ_{root_min}	Empirical minimal root-top (stem-base) pressure	Pa	
Φ_{s50}	Shape parameter—inflection point of stomata response to xylem pressure	Pa	
Ψ_0	Soil water potential when stomata or root are not limited by water availability	MPa	
Ψ_e	Soil water potential	MPa	
Ψ_w	Limiting soil water potential	MPa	

be applied solely to single trees. As a response to the need for a mechanistic approach that can be applied to entire ecosystems and coupled with land atmosphere models, we developed FETCH2, which allows the scaling of simulations to the plot scale and enables resolving xylem water potential and the corresponding tree hydraulic strategies at the regional and larger scales.

FETCH2 is an evolution upon its predecessor FETCH, [*Bohrer et al*., 2005]. To reduce simulation time and the inputs required regarding tree crown structure, it uses a finite difference numerical solver scheme and simplified one-dimentional (1-D) single beam conduit system. FETCH2 resolves processes at the resolution of an individual tree and subsequently scales representative single tree model output to the plot level based on the genus-size distribution of trees in a forest. The tree is represented as a single beam (i.e., "stem") with a realistic vertical leaf area distribution. The model is forced by atmospheric demand for water vapor and light availability to the leaves at each layer of the canopy, which are estimated using above canopy atmospheric conditions. The bottom boundary condition to the model represents the integrated effect of soil water availability on the water potential at the top of the root system. Table 1 includes a list of all symbols and units of the variables and parameters listed in the formulations and evaluation of the FETCH2 model (equation (1)–(20), below). The model code, set up to run an example using the parameters and site data from this study, is provided as supporting information to this manuscript (Dataset S3).

2.1.1. Governing Equations

Water pressure in the tree system, $\Phi(z, t)$, is resolved using equation (1) and updated at each time step, t, and at each vertical layer, z. This formulation represents a physically based approach to resolve water potential, which combines the continuity equation with a physical transport law applied to a stem segment, leading to a nonlinear partial differential equation, which resembles Richards' equation for soil water movement, including sources and sinks. In essence, this approach assumes that water movement through a collection of interconnected tracheids or xylem elements resembles porous media flow [*Chuang et al*., 2006; *Siau*, 1983; *Sperry et al*., 1998; *Sperry*, 2000]. The formulation of tree hydrodynamics we use here is based on the finite elements tree crown hydrodynamics (FETCH) model [*Bohrer et al*., 2005]. The key assumption of FETCH2 is that water transport is primarily driven by pressure and gravitational potential differences as opposed to other forcing, such as solute potential differences. In this equation and throughout the manuscript, subscript c represents the tree level, and subscript p represents the plot level. Superscript (c) indicates that the parameter or variable is genus specific. The change in xylem water potential is defined as follows:

$$C(z,t)^{(c)}\frac{\partial\Phi(z,t)}{\partial t}=\frac{\partial}{\partial z}\left[K(\Phi(z,t))^{(c)}\left(\frac{\partial\Phi(z,t)}{\partial z}-\rho g\right)\right]-\frac{El_c(z,t)}{\Delta z} \quad (1)$$

where $K^{(c)}$ and $C^{(c)}$ are the genus-specific conductivity and capacitance of the xylem, ρ is water density, g is gravity, and ρg represents the hydrostatic water potential.

The sink term $El_c/\Delta z$ is the simulated transpiration from each vertical layer of a particular tree crown at height z and time t. The transpirational water sink is determined using a response function, which limits the water loss through the stomata as a function of the nonhydrodynamically limited transpiration (NHL transpiration) and stem water potential. At each vertical element of the stem system, transpiration (El_c) is calculated by restricting the NHL transpiration (NHL_c) due to the hydrodynamic effects of xylem water potential. The second term in equation (2) mimics the stomatal regulation effect using an empirical response function of transpirational water loss related to stem water pressure at the previous time step:

$$El_c(z,t) = \mathrm{NHL}_c(z,t) \times \exp\left[-\left(\frac{-\Phi(z,t-1)}{\Phi_{s50}^{(c)}}\right)^{c_3^{(c)}}\right] \tag{2}$$

where $\Phi_{s50}{}^{(c)}$ is an empirical shape parameter describing the inflection point of the leaf stem water potential response curve. The time step difference between transpiration, El_c, and the xylem water pressure it responds to, $\Phi(z,t-1)$, is quasi-realistic as stomata do not respond instantaneously. Furthermore, this "lag time" allows greater numerical efficiency in the solution as it limits the implicit contribution of stem water potential to the water sink term. Our tests show that provided a reasonably small time step (order of minutes), it does not lead to numerical instability. The sensitivity of the response function of transpirational water loss (as defined by the parameters Φ_{s50} and c_3) determines the plant's leaf hydraulic strategy or expressed in another way the degree of (an)isohydric behavior.

Due to the characteristics of a porous medium, the conductivity and capacitance are not fixed properties but are dynamic functions of the water pressure (equations (3) and (5)). The relationship between water potential and conductivity is known as the xylem vulnerability or cavitation curve [*Sperry et al*., 2003]. Conductivity in unsaturated media drops rapidly with further decreases of water content. Plants have evolved to dynamically minimize the risk of cavitation by closing their stomata before critically low water contents are reached [*Sperry et al*., 1993; *Sperry*, 2003]. In FETCH2, xylem conductivity, $K^{(c)}$, is defined as follows:

$$K^{(c)}(\Phi(z,t)) = A_{\mathrm{Sap}}^{(c)} k_{\max}^{(c)} \exp\left[-\left(\frac{-\Phi(z,t)}{c_1^{(c)}}\right)^{c_2^{(c)}}\right] \tag{3}$$

where $A_{\mathrm{Sap}}{}^{(c)}$ is the stem cross-section area of active xylem of an individual tree. $k_{\max}{}^{(c)}$ is the maximum xylem conductance when it is saturated, and $c_1{}^{(c)}$ and $c_2{}^{(c)}$ are shape parameters of the cavitation curve.

Capacitance is defined using the formulation proposed by *Fatichi* [2014] based on the relationship between stem relative water content and water potential, RWC($\Phi(z,t)$), observed by *Barnard et al*. [2011] [see also *Domec and Gartner*, 2003].

$$\mathrm{RWC}(\Phi(z,t)) = 1 + \frac{\Phi(z,t)}{\left(b^{(c)}\Phi(z,t) - \phi_{z50}^{(c)}\left(2 + b^{(c)}\right)\right)} \tag{4}$$

The capacitance is a prognostic variable related to the water potential in the stem:

$$C(\Phi(z,t)) = \frac{A_{\mathrm{Sap}}^{(c)}}{V_{\mathrm{TOT}}}\frac{\mathrm{d}M_c}{d\Phi} = A_{\mathrm{Sap}}^{(c)}\left[\frac{\theta_{\mathrm{Sat}}^{(c)}A_{\mathrm{Sap}}^{(c)}\Delta z}{A_{\mathrm{Stem}}^{(c)}V_{TOT}}\left(\frac{-\phi_{z50}^{(c)}\left(2+b^{(c)}\right)}{\left(b^{(c)}\Phi(z,t) - \phi_{z50}^{(c)}\left(2+b^{(c)}\right)\right)^2}\right) + \frac{\rho}{X_E}\right] \tag{5}$$

where

$$b^{(c)} = \frac{\phi_{z88}^{(c)} - 0.24\phi_{z50}^{(c)}}{0.12\left(\phi_{z50}^{(c)} - \phi_{z88}^{(c)}\right)} \tag{6}$$

the term $\theta_{\mathrm{Sat}}{}^{(c)}A_{\mathrm{Sap}}{}^{(c)}\Delta z/A_{\mathrm{Stem}}{}^{(c)}$ represents the mass of water in the numerical stem segment, i.e., the element between each two nodes that result from the numerical discretization, when it is saturated, and is related to ratio between the cross-section area of the entire stem, $A_{\mathrm{Stem}}{}^{(c)}$, and the fraction of active xylem, $A_{\mathrm{Sap}}{}^{(c)}$.

FETCH2 is discretized in finite differences to be compatible with the numerical scheme of most land surface models. It resolves the water pressure in a 1-D single beam stem to reduce computational and data

requirements. A reduction in branching complexity was necessary because, while there are good sources of knowledge for stem height, diameter, and crown area from plot census and from remote sensing [*Garrity et al*., 2012], there is no good theory or data resource, to date, that allows generalizing and prescribing individual tree crown structures detailed to the branch level over a large scale that represent an entire forest area and region. Because the main purpose of FETCH2 is to introduce an approach for resolving aboveground water storage in trees for improvement of transpiration simulation in large-scale models, we deliberately reduced its complexity to the level that can be feasibly and realistically handled at these scales.

2.1.2. Forcing and Boundary Conditions

The FETCH2 model is forced by the tree level NHL transpiration NHL_c, at each vertical layer z, throughout the canopy. By our definition, NHL transpiration is the transpiration predicted considering the stomatal conductance as a function of atmospheric demand and photosynthetic capacity, but without any limiting effects of soil water availability (equation (7)). Most current models of transpiration can be used to generate NHL transpiration by simply removing the function that represents soil water availability limitations. We modified the formulation developed by *Ewers and Oren* [2000], which is driven by observed, half-hourly mean, gap filled, above canopy values of photosynthetically active radiation (PAR), air temperature (T_a), wind speed (u), and vapor pressure deficit (VPD):

$$\mathrm{NHL}_c(z,t) = \frac{A_{\mathrm{Crown}}{}^{(c)}\mathrm{LAI}_{\mathrm{Crown}}^{(c)}}{R\left(\frac{T_0}{T_a(t)+T_0}\right)\left(\frac{P(t)}{P_0}\right)} \times \left[\frac{\frac{g_b(u(z,t))\times g_s(\mathrm{PAR}(z,t),\,\mathrm{VPD}(t),\,T_a(t))}{g_b(u(z,t))+g_s(\mathrm{PAR}(z,t),\,\mathrm{VPD}(t),\,T_a(t))}\times \mathrm{VPD}(t)}{K_g(T_a(t))}\right] \tag{7}$$

where g_b is the leaf boundary layer conductance and is a function of wind speed (u) at canopy height z, and g_s is stomatal conductance and is a function of PAR, VPD and T_a at canopy height z, K_g is the conductance coefficient and is a function of T_a. $A_{\mathrm{Crown}}{}^{(c)}$ is the genus-specific mean crown area and $\mathrm{LAI}_{\mathrm{Crown}}{}^{(c)}$ is the genus-specific leaf area per crown area. A complete description of how multilayer NHL transpiration was computed (based on *Katul et al.* [2004] and *Poggi et al.* [2004]) is presented in Appendix A in the supporting information (Text S1.Appendix A).

A Neumann no-flux condition is prescribed at the topmost stem element such that water may only leave the stem through a sink term (in equation (1)) and not as a direct gradient flux:

$$\left.\frac{\partial \Phi}{\partial z}\right|_{z=z_{\mathrm{top}}} = 0 \tag{8}$$

A Dirichlet boundary condition is enforced at the base of the trunk, based on a Feddes-like [*Feddes et al*., 1976] formulation of soil moisture and rooting profile:

$$\Phi|_{t=0} = (1-\beta_s)\times\Phi_{\mathrm{root\_min}} = \left(1-\sum_e r_e\left(\frac{\Psi_w^{(c)}-\Psi_e}{\Psi_w^{(c)}-\Psi_0^{(c)}}\right)\right)\times\Phi_{\mathrm{root\_min}} \tag{9}$$

where β_s is the soil water stress function, Ψ_w is the limiting soil water potential, and Ψ_0 is the soil water potential when stomata or roots are not limited by water availability. Subscript e represents a particular vertical soil layer. r_e is the fraction of the root system in each soil layer e. In this work, we assumed the distribution of roots to be vertically uniform and used a single layer to represent the mean response from the surface to a depth of 30 cm where the soil moisture probes were installed [*Renninger et al*., 2014]. Ψ_w–Ψ_0 represents an empirical range of soil moisture within which stomata move from being fully open, to fully closed. $\Phi_{\mathrm{root\_min}}$ is an empirical minimal pressure (negative number) used to scale soil water potential to root-system-top xylem water potential, and can be determined from observations of the minimal predawn water potential, during days when the soil is extremely dry.

In the process of FETCH2 development, we chose to focus on aboveground hydrodynamic processes and show what improvements of ecosystem representation and accuracy in transpiration prediction are provided by resolving these processes. We treated all other processes that affect water fluxes as forcing using the same formulations commonly used in large-scale ecosystem models (here, represented by equation (7)). In order to allow an easier integration with large-scale ecosystem and Earth system models, we purposefully represented the effects of soil water availability through the Feddes approach, which is similar to almost all large-scale ecosystem and Earth system models representations [e.g., *Bonan*, 2002; *Fatichi et al*., 2012, 2016; *Ivanov et al*., 2012; *Janott et al*., 2011; *Siqueira et al*., 2008; *Sivandran and Bras*, 2013]. This does not imply that the

hydrodynamic processes at the soil-root interface are not important. In fact, one can easily claim that root water storage, root conductivity and structure, and other root processes such as hydraulic nighttime water redistribution and chemical controls all have important roles in the whole plant hydrodynamics. Additional improvements to tree water relations, which are beyond the scope of this study, can result from further improving the representation and resolution of soil-root processes. Examples of more sophisticated approaches to describe soil-root interface dynamics include *Bleby et al*. [2010], *Caldwell and Richards* [1989], *Domec et al*. [2004], *Doussan et al*. [2006], *Mackay et al*. [2015], *Verma et al*. [2014], *Bittner et al*. [2012], and *Vrugt et al*. [2001].

The simulations must be started before dawn, when an initial condition that prescribes hydrostatic pressure throughout the stem is realistic. Equations (1) through (9) form a closed set of equations, which can be solved numerically. Our finite difference discretization followed *Celia et al*. [1990]. The fully implicit Picard method and the backward Euler method were used to discretize spatially and temporally, respectively. The final equation was solved using a tridiagonal matrix algorithm. The detailed formulation of our numerical discretization and time integration approach is described in Appendix B in the supporting information (Text S1.Appendix B).

2.1.3. Hydrological Outputs of FETCH2

The model explicitly solves for the within-tree spatial and temporal dynamics of xylem water pressure. Equation (1), combined with the NHL transpiration (equation (7) and Appendix A in the supporting information Text S1) relates xylem water potential to transpiration. Besides xylem water potential and transpiration, FETCH2 also computes the aboveground water storage (S_c), and sap flux (J_c). The aboveground water storage of the stem (S_c) can be estimated from

$$S_c(t) = \sum_{z=z_{\text{bottom}}}^{z_{\text{top}}} (\text{RWC}(\Phi(z,t)) \times \theta_{\text{sat}} \times V_{\text{TOT}} \times \text{A}_{\text{Stem}}) \tag{10}$$

where z_{bottom} and z_{top} are the height at the base and top of the tree. Tree level sap flux (J_c) through the stem at each time step can be calculated through the water mass balance:

$$J_c(t) = \frac{(S_c(t) - S_c(t-1))}{\Delta t} + \sum_{z=z_{\text{bottom}}}^{z_{\text{top}}} El_c(z,t) \tag{11}$$

Tree level stem water storage can be inferred through in situ measurements of xylem RWC using frequency domain reflectometry [*Matheny et al*., 2015] or dendrometer-based approaches [*Steppe and Lemeur*, 2007]. J_c can be directly comparable with tree level sap flow observations. Storage and sap flux can be scaled to the plot level following section 2.5.

2.2. Study Site

The Silas Little Experimental Forest, also known as Rutgers University Pinelands Research Station, is located at northwestern part of the New Jersey Pine Barrens in Pemberton Township of Burlington County, NJ, USA (N 39°55′, W 74°36′). This study area is an oak/pine-dominated plot consisting of 58% chestnut oak (*Quercus prinus Willd*), 14% black oak (*Quercus velutina Lam*), 6% scarlet oak (*Quercus coccinia Münchh*), 8% scattered pitch pine (*Pinus rigida Mill*), 6% white oak (*Quercus alba L*), and 3% post oak (*Quercus stellata Wangenh*) [see *Schäfer et al*., 2010]. The species-specific leaf area index (LAI) was measured in the study site from 2005 to 2009 [*Schäfer et al*., 2014]. For the following years, we used the species-specific LAI litterfall campaign of 2009 in addition to the annual census data and revised the LAI of each species based on the percentage increment in the basal area. The canopy leaf area index (LAI) derived from litterfall was 1.7 in 2009. The composition and canopy LAI of the plot are reported on a yearly basis.

2.3. Site Level Observations

Methods for sap flux measurements and the meteorological observations at the study site are described in detail by *Schäfer et al*. [2014]. Half-hourly meteorological and flux data are available through the Ameriflux database (http://ameriflux.lbl.gov/), site-ID US-Slt. A complete data set of the observations used in this study, including sap flux, is available as supporting information to this manuscript (Dataset S1). The soil moisture content in the upper 30 cm of the soil was measured in four locations using CS616 sensors (Campbell Scientific Inc.). The sensors were attached to CR3000 datalogger (Campbell Scientific Inc.), which collected

data every 30 s and averaged data every 30 min [*Renninger et al*., 2014]. Flux measurements were conducted using the eddy covariance technique from a 19 m tower [*Clark et al*., 2012, 2010]. Total plot area of the study site is 0.3 ha, in which the tree and sapling diameters at breast height (DBH, cm) greater than 2.5 cm were measured at the end of each year from 2005 to 2013. For oak, sapwood area (A_{sap}, cm^2) was established based on the allometric relationships ($r^2 = 0.6$), determined by *Renninger and Schäfer* [2012], (equation (1)).

$$A_{Sap} = \pi \times SD(DBH - SD) \qquad \text{where} \quad SD = 0.0832 \times DBH \tag{12}$$

where SD is the sapwood depth of the tree individual in centimeter. For pine, we used the equation reported by *Renninger et al*. [2013] for calculating A_{sap} from DBH (equation (2), $r^2 = 0.99$).

$$A_{Sap} = 0.3733 \times DBH^{2.0473} \tag{13}$$

Species-specific and canopy total growing season LAI were provided by *Clark et al*. [2010] and *Schäfer et al*. [2010]. Realistic vertical distribution of leaf area density (LAD) was obtained for trees of the same genus in a similar plot in Michigan using a portable canopy LiDAR system [*Hardiman et al*., 2011].

2.4. Hysteresis Calculation

Despite being subjected to the same VPD, plants tend to transpire more during the morning hours, as compared to the afternoon, partially because of higher water storage in the stem during the morning hours, which becomes depleted later in the day [*Bohrer et al*., 2005; *Phillips et al*., 2003; *Verbeeck et al*., 2007a, 2007b]. Therefore, a hysteretic loop is created when transpiration is plotted against VPD during the course of a day [*Chen et al*., 2011; *O'Grady et al*., 2008]. This hysteretic loop depends on different factors including the time lag between daily maximum VPD and PAR and the hydrodynamic cycle of water storage within a plant. We define the magnitude of the hysteresis as the area enclosed by the daily hysteretic loop. The magnitude of the hysteresis was shown to be indicative of plant water status during the day and may be used to represent the hydrodynamic stress (expressed as the degree of imbalance between leaf water demand and soil water supply) incurred by the plant [*Matheny et al*., 2014a; *Novick et al*., 2014; *Zhang et al*., 2014]. We computed and analyzed the relative mean hysteresis of transpiration between genera. We calculated the mean hysteresis by normalizing daily transpiration and VPD by their respective daily maximum values, plotting the normalized transpiration against the normalized VPD and averaging this normalized daily hysteresis over all day with similar soil moisture conditions for the trees representing each genus.

2.5. Scaling to Plot Level

In order to efficiently scale individual-based FETCH2 simulations to a forest plot (corresponding, for example, to a grid cell of a coupled hydrologic or atmospheric model, or the footprint area of a flux tower), we followed the approach of *Matheny et al*. [2014b]. We classified the individual trees found in the forest census into groups according to their genus, resulting in two genus classes with a single size class. Predictions of tree level transpiration for each representative individual (El_c) were scaled to the plot level (El_p) using the following equation:

$$El_p(z,t) = \sum_c \lambda \frac{El_c(z,t)}{A_{Crown}^{(c)}} \frac{A_{Crown,tot}^{(c)}}{A_p} \tag{14}$$

where $A_{Crown}{}^{(c)}$ is the simulated tree's crown area, $A_{Crown,tot}{}^{(c)}$ is the total crown area of all the trees of that genus, A_p is the total plot area of the study site, and λ is the latent heat of vaporization. Sap flux at the plot level (J_p) can be derived from the tree level sap flux (J_c):

$$J_p(t) = \sum_c \lambda \frac{J_c(t)}{A_{Sap}^{(c)}} \frac{A_{Sap,tot}^{(c)}}{A_p} \tag{15}$$

where $A_{Sap}{}^{(c)}$ is the computed tree's sapwood area, $A_{Sap,tot}{}^{(c)}$ is the total sapwood area of all the trees of that genus. Plot level storage (S_p) is equal to the sum over all simulated trees of tree level stem water storage (S_c) divided by that tree's total occupied volume of the active xylem ($V_{TOT}{}^{(c)}$) multiplied by the total occupied volume of the active xylem for trees of that genus.

$$S_p(t) = \sum_c \frac{S_c(t)}{V_{TOT}^{(c)}} \sum_c V_{TOT}^{(c)} \tag{16}$$

Table 2. List of All the Parameters Selected for Calibration[a]

Parameter	Initial Values	Acceptable Range [Minimum, Maximum]	References	Optimized Parameters Oak	Optimized Parameters Pine
		Nonhydrodynamically Limited (NHL)[b]			
V_{cmax25}	40	[20, 85]	*Renninger et al.* [2015]	59.9	31.1
m	5	[4, 9]	*Renninger et al.* [2015]	6.7	7.3
x	4	[2, 6]		3.1	3.5
		FETCH2[c,d]			
		Stomata response to stem water potential[c]			
Φ_{s50}	-1×10^{5}	$[-2\times10^{6}, -1\times10^{5}]$	*Cruiziat et al.* [2002]	-9.1×10^{5}	-1.8×10^{5}
c_3	0.10	[0.1, 20]	*Cruiziat et al.* [2002]	12.3	10.3
		Xylem cavitation and capacitance curve[d]			
k_{max}	9×10^{-7}	$[9\times10^{-7}, 12\times10^{-6}]$	*Bohrer et al.* [2005]	1.6×10^{-6}	1.2×10^{-6}
c_1	1×10^{6}	$[1\times10^{6}, 2\times10^{6}]$	*Mayr et al.* [2003]	1.7×10^{6}	1.2×10^{6}
c_2	2	[2, 6]	*Chuang et al.* [2006]	3.0	2.8
ϕ_{x50}	-0.5×10^{6}	$[-6\times10^{6}, -0.5\times10^{6}]$		-2.5×10^{6}	-2.2×10^{6}
ϕ_{x88}	-0.1×10^{6}	$[-2\times10^{6}, -0.1\times10^{6}]$		-0.5×10^{6}	-0.5×10^{6}
		Soil water stress function[e]			
Ψ_0	−0.3	[−0.75, −0.3]	*Feddes et al.* [1978]	−0.51	
Ψ_w	−2.1	[−2.7, −2.1]	*Feddes et al.* [1978]	−2.56	
		Penman-Monteith + β		Optimized parameters Plot level	
V_{cmax25}	30	[20, 85]	*Renninger et al.* [2015]	55	
A	0.4	[0.4, 1.2]	*Feddes et al.* [1978]	0.8	
Ψ_0	−0.3	[−0.75, −0.3]	*Feddes et al.* [1978]	−0.64	
Ψ_w	−2.1	[−2.7, −2.1]	*Feddes et al.* [1978]	−2.49	

[a]References relate to selection criteria for acceptable ranges.
[b]Parameter type (1).
[c]Parameter type (2).
[d]Parameter type (3).
[e]Parameter type (4).

2.6. Parameter Estimation

We classify the FETCH2 model parameters into four distinct groups, based on the processes they affect:

1. *Transpirational demand parameters*. As described earlier and in Appendix A in the supporting information, the NHL transpiration is calculated through stomatal conductance for a given atmospheric condition while excluding limitations based on soil water availability. The physiological module of the NHL transpiration (equations (A.8)–(A.15) in Appendix A in the supporting information) has three different parameters: (1) V_{cmax}, the maximum carboxylation rate at 25°C [*Farquhar et al*., 1980], (2) m, the slope of the Ball-Woodrow-Berry stomatal conductance model [*Ball et al*., 1987], and (3) x, ratio of horizontal to vertical projections of leaves.
2. *Stomatal response parameters*. This set determines the shape and sensitivity of the stomatal response to stem water potential: Φ_{s50} and c_3, which define the simulated tree's hydraulic strategy on the isohydric-anisohydric continuum (equation (2)).
3. *Xylem hydraulics parameters*. The xylem cavitation curve and water storage capacity are described by k_{max25}, θ_{Sat}, c_1, c_2, $\phi_{z,50}$, and $\phi_{z,88}$ (equations (3)–(5)). We expect these parameters to define specific xylem architectures, for example, nonporous, diffuse-porous, or ring-porous xylem as well as the degree of coupling between xylem conduits and storage tissues.
4. *Soil water availability regulation parameters*. Φ_{root_min}, r_e, and β_s determine root-depth distribution, the relationship between soil water potential in the root zone and stem-base water potential, and the soil water stress function (equation (9)). These parameters can be modified to represent the rooting depth as well as other root strategies that affect water availability such as rooting vertical distribution, rooting length and diameter, and efficiency of water extraction.

Among all the parameters defined in FETCH2 formulations, we chose to perform the model calibration on the parameters listed in Table 2. This selection was carried out based on the predicted sensitivity of the model

outputs (simulated transpiration and sap flux) to the selected parameters, which was evaluated by reviewing the literature and from some preliminary model simulations. The initial values and ranges of these parameters along with their corresponding references are listed in columns 2, 3, and 4 of Table 2. For this study we used only one soil layer, such that the root distribution function was equal to 1 ($r_e = 1$). The discrete spatial and temporal increments used to numerically solve equation (1) were fixed and did not change throughout the simulation or the stem model, with $\Delta z = 200$ mm and $\Delta t = 180$ s.

As is customary with land atmosphere and ecosystem models such as Community Land Model [*Bonan et al*., 2002], ED2 [*Medvigy et al*., 2009], and T&C [*Pappas et al*., 2016], we assume that the aforementioned physiologic and hydraulic parameters (Table 2) are not age/size-specific but are properties of the plant functional type or species (in this study represented as two different genera). Therefore, we parameterized the genus-specific NHL and FETCH2 formulations through an optimization algorithm considering a predefined objective function, which includes the measurement of latent heat flux. We used a two-step parameterization process. First, we calibrated the NHL transpiration (forcing), using the sum of squared error between the NHL transpiration and observed plot level transpiration as an objective function. Derivation procedures of the observed plot level transpiration are outlined in the following paragraph. Optimizing the NHL transpiration guarantees that any further improvement to the simulated transpiration by FETCH2 relative to the NHL transpiration model is a result of the improved dynamics in FETCH2 and not an artifact of poor parameterization of the NHL transpiration model. Next, we used the parameterized NHL transpiration component to optimize the other FETCH2 parameters, based on the double exponential error distribution.

The NHL calibration required determination of the plot level observed transpiration ($EOBS_p$) from the observed plot level latent heat flux (evapotranspiration, $LEOBS_p$) using the approach introduced by *Williams et al*. [2004]. This approach assumes that during dry conditions the differences between the eddy covariance observed latent heat flux ($LEOBS_p$) and transpiration approximated through plot-scaled sap flux ($JOBS_p$, scaled from tree level observed sap flux ($JOBS_c$) using equation (15)) correspond to errors in sap flux scaling. However, during nonwater-limited conditions and shortly after precipitation events, the deviations between scaled sap flux and $LEOBS_p$ are the result of the inclusion of evaporation from the soil and intercepted-precipitation in $LEOBS_p$ [*Williams et al*., 2004]. The ratio of evapotranspiration/transpiration calculated for this study site was, on average, 70% during 2009 and 65% during 2011.

The FETCH2 parameterization was performed using a delayed rejection-adaptation Markov-Chain Monte Carlo-Metropolis Hasting algorithm (MCMC-MH). This approach is a modified version of the adaptive MCMC algorithm [*Haario et al*., 2006, 2001], which tends to improve the convergence efficiency of the algorithm. The algorithm assumes Gaussian distribution for each of the parameters. In the first iteration, MCMC creates a prior distribution for each parameter assuming infinite variance and the mean equal to expected value of the initial parameter (Table 2). The distribution is updated at each iteration adaptively considering the mean at current point and covariance determined by the spatial distribution of the parameter states [*Haario et al*., 2001].

The MCMC technique evolves the parameter values iteratively until the distribution associated with each optimized parameter converges to a stable posterior distribution. The optimum parameter set is selected as the parameter set that maximizes the likelihood. The MCMC algorithm requires the user to pick initial, lower bound, and upper bound values for each of the parameters to be optimized and the maximum number of iteration for the sampling process. We set the algorithm to run for 1000 iterations, 200 of which are discarded as burn-in. The initial, lower bound, and upper bound values for the parameters were determined based on the existing literature (columns 2 and 3, Table 2). There are different methods to ensure that the algorithms have found a true global optimum [*Brooks and Roberts*, 1998]. In this study, we used a "burn-in" method, which rejects a certain fraction of the neighborhood explorations before accepting points.

2.7. Evaluation of Model Performance

The Penman-Monteith (PM) model [*Monteith*, 1965; *Penman*, 1948; *Thom*, 1972] is a widely used evapotranspiration model that does not include any mechanistic link between soil water potential and stomatal conductance (Appendix C in the supporting information Text S1) [*Ershadi et al*., 2014; *Stannard*, 1993]. The PM model was driven by the atmospheric forcing including net radiation, ground heat flux, VPD, wind speed, humidity, and temperature and calculates the plot level expected evapotranspiration. We parameterized the PM model

Table 3. Site-Specific Atmospheric and Soil Properties During the Experiment's Period in 2009 and 2011

Month	Average of Maximum Daily VPD (kPa)	Mean Wind Speed (ms^{-1})	Mean Air Temperature (°C)	Average of Maximum Daily PAR ($\mu mol\, m^{-2}s^{1}$)	Mean Soil Moisture (%)	Total Precipitation (mm)
			2009			
June	1.5	1.4	19.6	1488	8.1	104.6
July	2.2	1.5	22.4	1683	6.9	121.8
August	2.1	1.2	23.7	1560	7.8	133.8
			2011			
June	2.3	1.4	22.3	1681	5.4	38.9
July	2.8	1.4	25.5	1691	6.3	121.9
August	2.1	1.5	22.7	1509	8.7	370.8

using the half-hourly transpiration derived from the observed latent heat flux using *Williams et al*. [2004] (Table 2), assuming that transpiration is the primary component of evapotranspiration in PM model.

To demonstrate how well the mechanistic representation of tree hydrodynamics by FETCH2 improves the simulation of transpiration beyond current, broadly used transpiration models, we compared the FETCH2 predictions of plot level transpiration with the plot level transpiration determined by the parameterized NHL and PM models. To make this comparison meaningful, we incorporated the direct soil water limitation effect on the stomatal conductance of the NHL and PM models by multiplying their resolved stomatal conductance by the soil water stress function (β_s) (equation (9)).

We used four different performance metrics to evaluate the models: (1) coefficient of determination (R^2); (2) Bias (B), which is the average difference between observation and simulation; (3) normalized mean absolute error (NMAE) [*Medlyn et al*., 2005]:

$$\mathrm{NMAE} = \sum_t \frac{\mathrm{EOBS}_p(t) - E_{\mathrm{sim}}(t)}{n\overline{\mathrm{EOBS}_p(t)}} \tag{17}$$

where EOBS_p is the observed plot level transpiration and E_{sim} is the model-simulated transpiration. The over bar indicates averaging across all values of observations (n is the number of observations). Finally, (4) reduced χ^2 statistic [*Taylor*, 1982]:

$$\chi^2 = \frac{1}{n}\sum_t \left(\frac{\mathrm{EOBS}_p(t) - E_{\mathrm{sim}}(t)}{2\sigma_{\mathrm{obs}}}\right)^2 \tag{18}$$

where σ_{obs} is the standard deviation of the observations. In this formulation, the coefficient 2 in the denominator normalizes the uncertainty of observed values (EOBS_p) to account for the 95% confidence interval. χ^2, indicates the model-data mismatch along the range from 0 to infinite. Values of χ^2 close to 1 indicate that model result and observations are in agreement relative to existing uncertainty in observations.

Akaike information criteria (AIC) is a leading method for selecting the best model among several competing models. This selection criterion was based on a combination of model's goodness of fit (penalized likelihood) and number of parameters. AIC is defined as [*Akaike*, 1974; *Burnham and Anderson*, 2002] follows:

$$\mathrm{AIC}_f = -2\times\left(\ln\left(\left(2\pi\sigma^2\right)^{-n/2}\exp\left(-\frac{1}{2\sigma^2}\sum\left(\mathrm{EOBS}_p - E_{\mathrm{sim}}\right)^2\right)\right)\right) + 2\times NO \tag{19}$$

where σ^2 is the variance of the error term, and NO is the number of free parameters in the model. In the scope of comparing various models, the relative probability that a model f minimizes the estimated information loss (RL_f) is defined as [*Burnham and Anderson*, 2002] follows:

$$\mathrm{RL}_f = \exp\left(\left(\mathrm{AIC}_{\min} - \mathrm{AIC}_f\right)/2\right) \tag{20}$$

where $\mathrm{AIC}_{\min}$ is the minimum AIC_f and AIC_f is the Akaike information number for model f. The minimum AIC, corresponds to the model with the best performance for which RL_f is equal to 1.

Table 4. Average of Main Attributes of the Existing Genera (Oak/Pine) at Silas Little Experimental Forest, New Jersey[a]

PFT	$DBH^{(c)}$ (cm)	$z_{top}{}^{(c)}$ (m)	$A_{Sap}{}^{(c)}$ (cm^2)	$A_{Crown}{}^{(c)}$ (m^2)	$A_{Sap,tot}{}^{(c)}$ (m^2)	$A_{Crown,tot}{}^{(c)}$ (m^2)
			2009			
Oaks	19.7	12.0	99	28.8	0.20	10239
Pines	35.9	17.0	509	46.1	0.05	1290
			2011			
Oaks	18.3	12.0	88	28.8	0.18	7370
Pines	37.3	17.0	616	46.1	0.06	1325

[a]The first four attributes are averages of the trees with sap flow measurements.

2.8. Site-Specific Simulation Setup

We chose the peak-growing season (1 June to 31 August) of 2009 to perform the calibration on PM, NHL, and FETCH2 models. Then, we evaluated the performance of the parameterized models using the observed data collected during the peak growing season of 2011. Meteorological data, including humidity, wind speed, air temperature, PAR, and atmospheric pressure, were gap filled using bilinear, periodic trended interpolation [*Morin et al*., 2014]. Flux data, including sap flux and latent heat fluxes, were gap filled using the artificial neural network (ANN) method, which is a common approach to gap filling of flux data [*Papale et al*., 2006]. The ANN's specific setup applied in our study is described in detail in *Morin et al*. [2014]. In this study, 26.5% of the 2009 and 26.7% 2011 latent heat fluxes were gap filled using the ANN method. In addition, to assure the accuracy of our parameterization, days with more than eight sequentially missing half-hourly sap flux observations were removed from the optimization process.

Table 3 includes the average of maximum daily VPD, mean wind speed, mean air temperature, average of maximum daily PAR, mean soil moisture, and total precipitation for the selected simulation periods in 2009 and 2011.

Simulations were performed at the genus level using a single representative tree for each genus. $DBH^{(c)}$, height ($z_{top}{}^{(c)}$), sapwood area ($A_{Sap}{}^{(c)}$), crown area ($A_{Crown}{}^{(c)}$) of a representative "average tree," total sapwood area of the trees with sap flow measurement ($A_{Sap,tot}{}^{(c)}$), and total crown area ($A_{Crown,tot}{}^{(c)}$) of the two existing genera (oak/pine) in 2009 and 2011 are presented in Table 4.

3. Results and Discussion

3.1. Model Performance Evaluation

We calibrated the PM and NHL models based on observed half-hourly transpiration and FETCH2 based on observed half-hourly sap flux. We used the MCMC algorithm to optimize NHL and FETCH2 parameters for each of the two genera (oak and pine) and for the PM model for the whole plot. The resulting calibrated PM, NHL, and FETCH2 parameters are listed in Table 2. We used these parameters to represent the

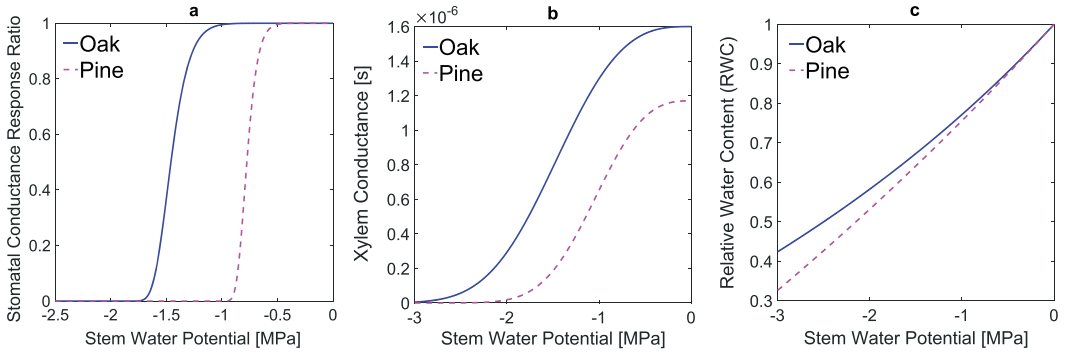

Figure 1. Differences in hydraulic traits between the oaks and pines predicted by our optimized FETCH2: (a) Stomata response curve describing leaf response to stem water potential, (b) Xylem conductance, and (c) Stem capacitance—relative water content (RWC) response to changes in the stem water potential for the parameterized oak (solid line) and parametrized pine (dashed line). We plotted the curves over an arbitrary range of stem water potential with the optimized parameters from Table 2 to compare the hydraulic properties of the two existing genera qualitatively.

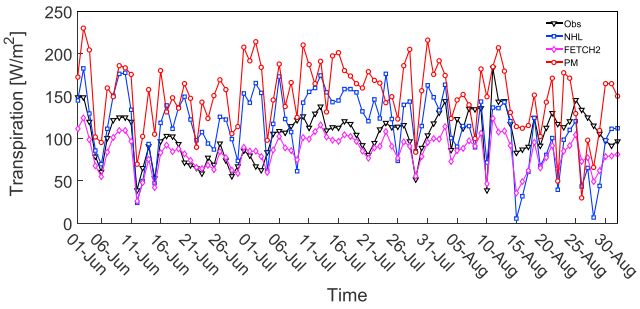

Figure 2. Mean daily plot level NHL (blue square), FETCH2 (magenta diamond), Penman-Monteith (red circle), and observed (black triangle) transpiration.

hydrodynamic variables of FETCH2 for both genera including stomatal response ratio, (the ratio of FETCH2 simulated water-limited transpiration sink (El_c) to NHL transpiration forcing (NHL_c)), xylem conductance (k), and finally the RWC (equation (4)).

Figure 1 illustrates how genera-specific parameterizations reflect the differences between oaks' and pines' hydrodynamic properties and hence the hydraulic strategies of the two genera. With the onset of water stress, i.e., the initial drop in stem water potential, the oak maintains higher stomatal conductance as compared to the pine (Figure 1a). This characterizes oak as the more anisohydric of the pair. The oak, having higher maximum xylem conductance (k_{max}, Table 2), maintains a higher conductance within the displayed range of stem water potential deficit. Changes in relative stem water content per stem water potential are similar between oak and pine, but pine tends to release more water (lower RWC) for the same drop in water potential (Figure 1c).

3.2. Model Evaluation

We simulated the tree level NHL transpiration in 2011 and used it to force the parameterized FETCH2. Figure 2 illustrates the mean daily dynamics at plot level of observed and simulated transpiration with NHL, FETCH2-resolved, and Penman-Monteith models.

Figure 2 visually demonstrates that the mean daily plot level transpiration, simulated by FETCH2, is closer in value to the mean daily observed transpiration compared to the other two models. To compare the differences between models, model skill metrics (section 2.7) were evaluated based on the magnitude of transpiration hysteresis and half-hourly and mean daily transpiration for all the three models (Table 5).

FETCH2 outperforms both the optimized NHL and PM models for simulations of transpiration at the half-hourly and daily scale and for simulations of the hysteresis of transpiration. The NMAE and χ^2 criteria for FETCH2 were closer to zero and unity, respectively. This indicates that FETCH2 has significantly improved the simulation of transpiration through the incorporation of within-tree hydrodynamic processes, rather than only considering the soil moisture limitations. Simulated NHL transpiration displayed better performance compared to PM, particularly at the half-hourly scale.

Table 5. Performance Metrics of NHL Model, FETCH2, and Penman-Monteith Based on Plot Level Transpiration Hysteresis and Half-Hourly and Mean Daily Simulations of Transpiration (the Bold Numbers Are the Performance Metrics That Have Been Improved by FETCH2 Simulation)

Models	NMAE	χ^2	B	R^2
		Hysteresis		
NHL	0.279	10.696	0.146	0.59
FETCH2	**0.062**	**2.566**	**−0.133**	**0.91**
PM	0.373	19.207	0.165	0.32
		Half-Hourly Simulation of Transpiration		
NHL	−0.094	5.822	10.873	0.75
FETCH2	**0.0098**	**0.724**	**−0.002**	**0.93**
PM	−0.368	90.609	0.565	0.45
		Mean Daily Simulation of Transpiration		
NHL	−0.093	2.880	67.791	0.58
FETCH2	**0.0619**	**1.270**	**−6.663**	**0.78**
PM	−0.367	44.118	50.117	0.36

Table 6. Comparison Between the Akaike Information Criteria (AIC) and Relative Likelihood of NHL, PM, and FETCH2 Models

Model	Akaike Information Criteria (AIC)	Relative Likelihood (RL)
NHL	26.35	0.11
PM	74.28	4.28×10^{-12}
FETCH2	**21.89**	**1**

Although the performance metrics in Table 5 showed that FETCH2 improves the NHL simulation of transpiration, since these three models use different numbers of parameters, we used AIC and RL statistics to analyze the effect of overparameterization. Considering that the NHL model has 3, the PM model has 4, and the FETCH2 model has parameters that were calibrated, we calculated the AIC and RL numbers for each of the three transpiration models using the Gaussian distribution of the likelihood (Table 6).

Despite having more free parameters, FETCH2, with the lowest AIC number, has the highest probability to minimize the modeling error. The NHL model is 0.11 times, and the PM model is 4.28×10^{-12} as probable as FETCH2 to minimize the simulation error, confirming the advantage of the hydrodynamic approach.

We categorized the days within the simulation period (1 June to 31 August 2011) into three groups: wet (with daily mean soil moisture larger than 10%), intermediate (with daily mean soil moisture between 5% and 10%), and dry days (with daily mean soil moisture less than 5%). For each category, we calculated the relative hysteresis of transpiration (section 2.4). Figure 3 shows the mean relative hysteretic loop for days with intermediate soil moisture, created based on the observed and simulated (FETCH2, PM, and NHL) transpirations. Similar to the performance metrics presented in Table 5, Figure 3 also shows that FETCH2 performed better than the two other models in predicting the magnitude of hysteresis. Neither the PM nor the NHL models are able to reproduce the hysteresis of transpiration as accurately as FETCH2 (Figure 3).

One of the outputs of FETCH2 is sap flux. This is advantageous in cases where direct observations of sap flux exist as an additional variable for model evaluation. Figure 4 shows the total daily tree level observed and FETCH2 simulated sap flux for both oak and pine with a very good agreement.

Figure 5 shows the daily dynamics of the observed soil moisture, tree level simulated stem water storage, and observed and simulated water fluxes (sap flux and transpiration) within a selected period of 10 consecutive days during a drying period, with initially high and gradually declining soil moisture. FETCH2 successfully captured the interdaily and intradaily pattern of water flux. FETCH2 predicts higher transpiration rates before noon than afternoon, with the diurnal transpiration curve gradually skewing toward the morning, as the soil becomes dryer and overall daily transpiration declines. The model also shows the diurnal dynamics of stem water storage depletion and nighttime recharge.

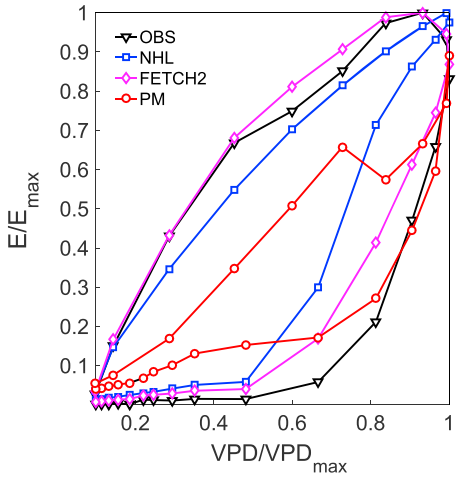

Figure 3. Mean hysteresis loop of observed (black triangle), NHL (blue square), FETCH2 (magenta diamond), and PM (red circle) simulated transpirations under intermediate soil moisture condition.

3.3. Identifying Differences in Hydraulic Strategies Between Oak and Pine

Plants lose water from storage in the stem and branches during the morning due to faster rate of water loss through transpiration than recharge of the stem xylem [*Matheny et al.*, 2015]. Some trees may reduce their stomatal conductance during and after peak water demand (at midday and early afternoon) by closing the guard cells to prevent further water loss and drop of water potential in the plant [e.g., *Sack and Holbrook*, 2006]. This process is called "midday stomata closure" [*Manzoni et al.*, 2013; *Sperry et al.*, 1993, 2002] which affects the diurnal dynamics of transpiration as well as the long-term totals of

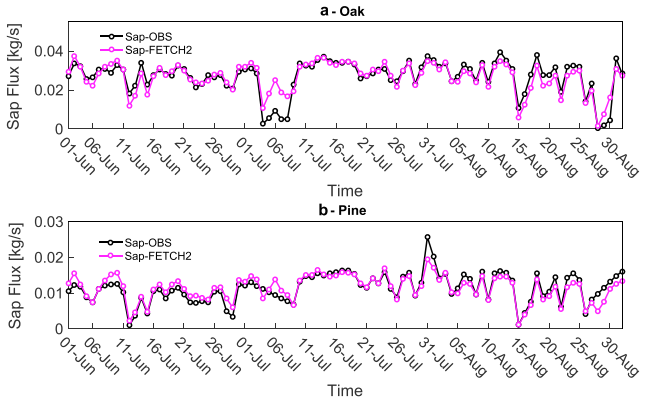

Figure 4. Total daily tree level observed (black) and FETCH2-simulated (magenta) sap flux during the simulation period for (a) oak and (b) pine.

transpired water and through its dependence on stomatal conductance, affects carbon fluxes as well.

One of the advantages of FETCH2 is the ability to resolve differences among trees with various hydraulic strategies through multiple parameters that are not typically resolved by other models (Table 2). Genus-specific parameterization of FETCH2 yields groups of parameters that can effectively characterize the hydraulic strategy of the genera. The FETCH2 model represents stomatal-response sensitivity to stem water potential through two parameters: Φ_{s50} and c_3 (Table 2 and Figure 1a), thus characterizing the relatively anisohydric strategy of oaks versus the more isohydric strategy of pines (Figure 1).

Renninger et al. [2014] and *Renninger et al*. [2015] showed that pine trees in the Silas Little experimental forest demonstrate a relatively isohydric response. As shown in Figure 1a, we determined that stomatal response occurs over a range of less negative stem water potentials for pine (e.g., steeper decline in the stomatal response ratio) than for oak. This indicates that the transpiration rate is more vulnerable to drops in stem water potential and, over a large range of water potentials, a lower value of stomata conductance (corresponding to actual transpiration) will be obtained for pine than for oak at the same xylem water potential.

Responses to changes in soil water availability depend on the tree's hydraulic strategy [*Tardieu and Simonneau*, 1998]. Anisohydric plants experience larger leaf water deficits at midday during dry soil water conditions than in wetter conditions. Isohydric plants demonstrate less variability between midday leaf water potential during dry and wet conditions, mainly due to the strong downregulation of their transpiration under dry conditions. Similar to Figure 3, we categorized the days into dry, intermediate, and wet days and calculated the normalized mean daily transpiration for each one of these categories.

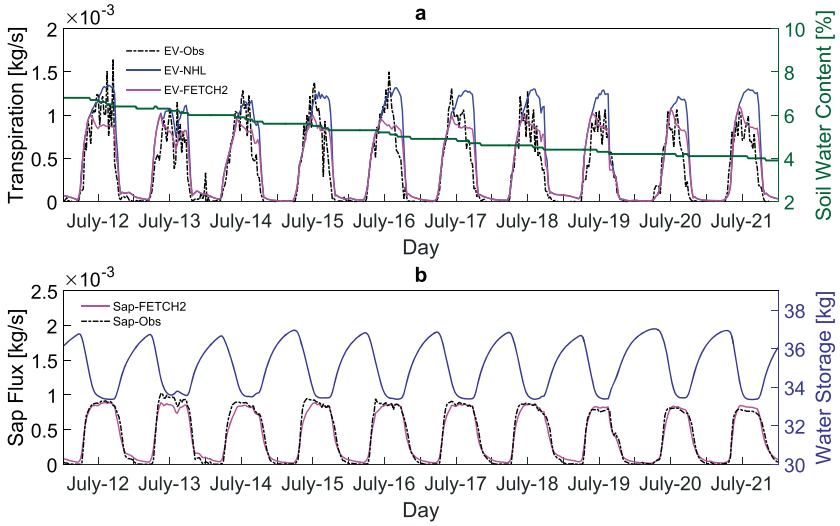

Figure 5. Ten days dynamics of (a) left y axis: Oak's tree level NHL (solid blue line), FETCH2-simulated (solid magenta line), and observed (dashed dot black line) transpiration, right y axis: soil water content (solid green line), (b) left y axis: Oak's tree level observed (dashed black line), and FETCH2-simulated (solid magenta line) sap flux, right y axis: Oak's water storage (solid blue line).

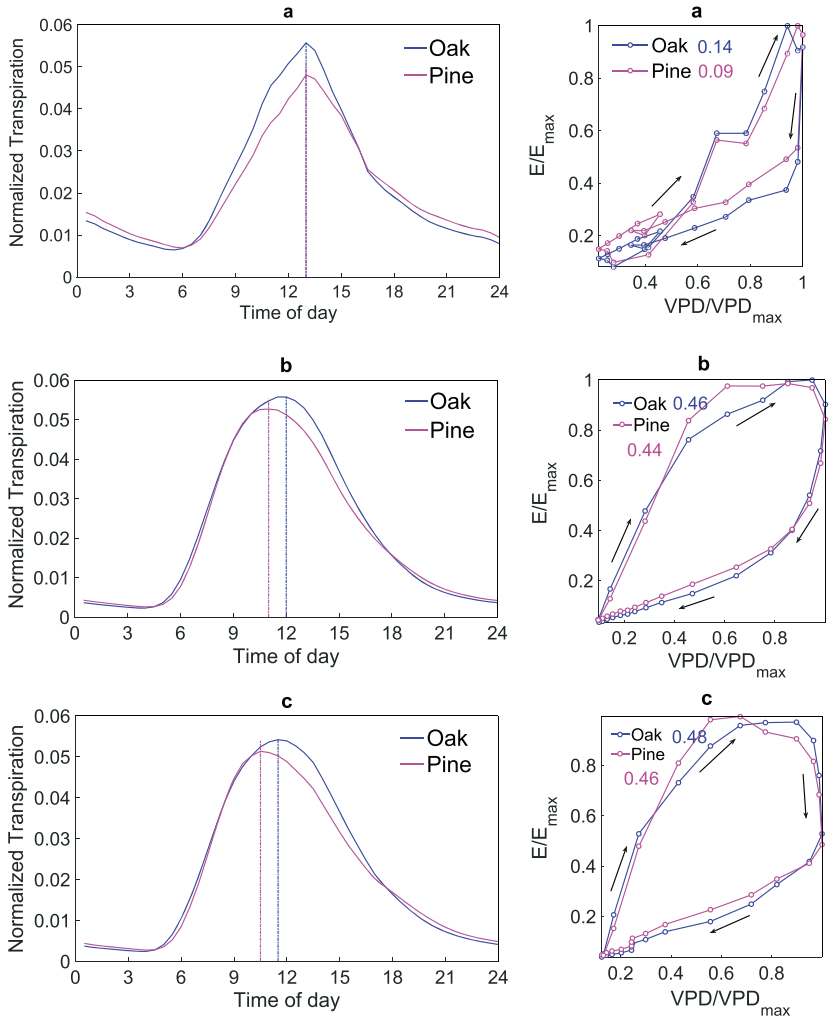

Figure 6. (left column) Normalized (with respect to total daily) mean daily cycle of transpiration during (a) wet days, (b) intermediate soil moisture, and (c) dry condition for oak (solid blue line) and pine (solid magenta line). The blue and magenta dashed lines represent the peak of normalized transpiration. (right column) Relative mean hysteresis loop of transpiration with their corresponding hysteresis values, during (a) wet days, (b) intermediate soil moisture, and (c) dry condition for oak (solid blue line) and pine (solid magenta line). Hysteresis was calculated using the method explained in section 2.7.

Both oak and pine reach their maximum daily transpiration rate around noon under wet conditions (Figure 6a). Under the intermediate conditions, both genera peak earlier; however, pine appears to be more sensitive to the drying soil conditions and reaches its peak transpiration rate earlier in the morning (Figure 6b). Pine shifts its peak transpiration earlier, to around 10 am, under extremely dry conditions, while oak transpiration continues to peak around 11 am (Figure 6c). Therefore, soil water limitations play a smaller role in regulating oak transpiration than for other, more isohydric species such as pine.

We conducted a paired sample *t* test to determine whether there are any significant differences between daily absolute hysteresis means of oak and pine. We performed the test separately for each soil moisture condition. The test result revealed that there are statistically significant differences between oak's and pine's daily absolute hysteresis ($p < 0.0001$) in all three soil moisture conditions, while oak maintains higher daily hysteresis of transpiration. This confirms the results of *Matheny et al*. [2014b], who showed that a ring porous anisohydric species of oak, *Quercus rubra*, demonstrated larger mean relative hysteresis as compared to similarly sized isohydric species. We speculate that in order to reduce the effect of soil water stress, oak must either draw water from deeper layers, be more conductive and efficient in overnight recharge, and/or have a more effective hydraulic redistribution than pine [*Robinson et al*., 2012].

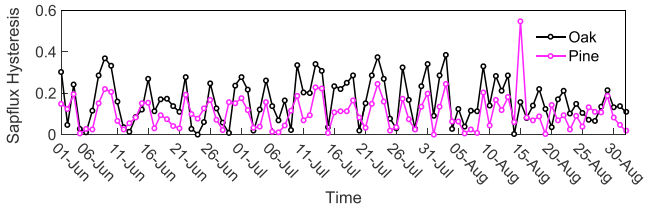

Figure 7. Dynamics of diurnal relative hysteresis of tree level sap flux for oak (black) and pine (magenta).

Similarly to transpiration, sap flux also exhibits diurnal hysteresis that is illustrated by plotting the normalized simulated sap flux as a function of normalized VPD during the course of each day [*Chen et al*., 2011; *O'Grady et al*., 2008]. Figure 7 shows that throughout the simulation period, oak maintains a larger degree of daily sap flux hysteresis as compared to pine. The diurnal hysteresis of sap flow can be indicative of the diurnal hydrodynamic stress on plants [*Matheny et al*., 2014b]. Mechanistically, the differences in the vessel and intervessel pit structure of plant species cause a trade-off between the water transport capacity ("efficiency") and safety among plants [*Manzoni et al*., 2013]. The efficiency of plant species can be characterized by the maximal hydraulic conductivity. High efficiency if often obtained at the cost of larger vulnerability to cavitation (less negative values of water potential at 50% loss of conductivity). "Safety" is characterized by lower xylem conductivity but larger resistance to cavitation, or higher margin between minimum water potentials during droughts and critical cavitation levels [*Manzoni et al*., 2013; *Meinzer et al*., 2010]. Thus, oak, by being on the efficiency side of the "safety-efficiency" continuum and experiences stronger depletion of stem-water storage, requires more time to replenish its water storage and hence has relatively lower sap flux in the afternoon compared to more isohydric species like pine [*Manzoni et al*., 2013; *McCulloh et al*., 2012; *Taneda and Sperry*, 2008; *Tyree and Zimmermann*, 2002]. Pine, on the other hand, as an isohydric coniferous genus demonstrates less sap flow hysteresis [*Matheny et al*., 2014b; *McAdam and Brodribb*, 2014].

Xylem architecture is one of the factors that imposes physical limitation on the water transport rate within a tree, and its variations across species can explain some of their water use strategies [*Bush et al*., 2008; *Lens et al*., 2011; *Sperry et al*., 2002; *Thomsen et al*., 2013]. Wood anatomy affects wood traits such as xylem conductivity (K) and xylem capacitance (C). For example, the ring-porous oak with wide vessels in the wood structure results in higher conductivity during the high water availability condition yet decreases the safety margin of these species during drought [*Bovard et al*., 2005; *Hacke et al*., 2001; *Taneda and Sperry*, 2008; *Thomsen et al*., 2013]. This structure causes the plant to be more conductive but also more vulnerable to cavitation under water limiting conditions.

However, interactions with leaf traits, which in this case were more isohydric for pines versus anisohydric for oaks, and potentially additional interactions with root traits, such as rooting depth, can lead to a whole-plant level strategy that does not necessarily present the vulnerabilities expected by the xylem structure only. We suggest that these multitrait whole-plant level combined hydrodynamics may explain the fact that only weak evidence for the safety-efficiency trade-off was found when studying only xylem traits in many plant species [*Gleason et al*., 2016]. For example, in the case we studied, the generally more conductive xylem of oaks allowed maintaining high transpiration rates despite decreasing midday xylem-water potentials without signs of widespread cavitation.

4. Conclusion

We demonstrated that FETCH2 can effectively represent the continuum of hydraulic properties of stems and leaves over different genera with a wide range of characteristics through its parameterization process as depicted by the differences between wood properties of oak and pine. By incorporating the consequences of tree-water storage and hydraulic strategy in regulating stomatal conductance, the hydrodynamic modeling approach that we presented here may have a large impact on revising the structure of hydrologic, land surface models, DGVM, and coupled Earth system models. Simulating the aboveground water storage in trees enhances our understanding of the role hydrodynamic limitations and intradaily water stresses play on transpiration. By accounting for tree hydrodynamics, FETCH2 is able to resolve the outcomes of different hydraulic strategies. The difference in the parameter values that represent the traits in FETCH2 corresponds to the different trees' hydraulic strategies—namely, the continuum between isohydric and anisohydric regulation

of stomatal conductance. Through the parameterization process, FETCH2 has the ability to capture differences in xylem anatomy such as conductivity and capacitance of the xylem. By resolving aboveground stem water flow, storage and potential, it can effectively describe the difference in hydraulic strategies between plants.

The genus-specific parameterization of FETCH2 illustrates that with the same drop in xylem water potential, oak maintains higher stomatal conductance, higher xylem conductance, and higher RWC than pine. The model simulations demonstrated that soil water limitations play a smaller role in regulating oak transpiration than for the more isohydric species, pine, under nearly all water availability conditions. In response to the same changes in soil water availability, oaks experienced larger xylem water deficits at midday during dry soil water conditions compared to the wetter conditions but maintained high transpiration rates. As expected for a more isohydric species, pine demonstrated less variability between midday leaf water potential during dry and wet conditions but downregulated transpiration, and closed stomata earlier during the day when the soil was dry. We showed that the diurnal dynamics of transpiration for each genus shows a characteristic and different response to increasing soil moisture stress. These responses integrate at the plot level to a combined diurnal and overall transpiration dynamics that were not easily predictable by nonhydrodynamic models of transpiration, which do not resolve aboveground water storage and its effects. Application of this modeling approach in other mixed forests with trees of different hydraulic strategies will result in better estimation of the plant contribution to the land surface energy balance and therefore a more accurate assessment of water resources and carbon uptake rates.

Acknowledgments

Funding for this study was provided by the U.S. Department of Energy's Office of Science, Ameriflux core site program, Office of Biological and Environmental Research, Terrestrial Ecosystem Sciences program award DE-SC0007041. National Science Foundation Hydrological Science grant 1521238. Support for A.M. Matheny was provided by the Ohio State University Presidential Fellowship and the P.E.O. Scholar Award. The model code, the half-hourly sap flux data and tree-plot scaling data are provided as supporting information to this manuscript (Dataset S3, Dataset S2, resectively). Half-hourly meteorological and latent heat flux data are included as supporting information (Dataset S1) and are also available through the Ameriflux database (http://ameriflux.lbl.gov/). Any opinions, findings, and conclusions or recommendations expressed in this material are those of the authors and do not necessarily reflect the views of the funding agencies.

References

Akaike, H. (1974), A new look at the statistical model identification, *IEEE Trans. Autom. Control*, *19*(6), 716–723, doi:10.1109/TAC.1974.1100705.

Anderegg, W. R., J. A. Berry, D. D. Smith, J. S. Sperry, L. D. Anderegg, and C. B. Field (2012), The roles of hydraulic and carbon stress in a widespread climate-induced forest die-off, in *Proceedings of the National Academy of Sciences*, edited by Stephen W. Pacala, pp. 233–237, Princeton Univ., Princeton, N. J., doi:10.1073/pnas.1107891109.

Ball, J. T., I. E. Woodrow, and J. A. Berry (1987), A model predicting stomatal conductance and its contribution to the control of photosynthesis under different environmental conditions, *Prog. Photosynth. Res.*, *4*, 221–224.

Barnard, D. M., F. C. Meinzer, B. Lachenbruch, K. A. McCulloh, D. M. Johnson, and D. R. Woodruff (2011), Climate-related trends in sapwood biophysical properties in two conifers: Avoidance of hydraulic dysfunction through coordinated adjustments in xylem efficiency, safety and capacitance, *Plant, Cell Environ.*, *34*(4), 643–654, doi:10.1111/j.1365-3040.2010.02269.x.

Bittner, S., M. Janott, D. Ritter, P. Köcher, F. Beese, and E. Priesack (2012), Functional–structural water flow model reveals differences between diffuse-and ring-porous tree species, *Agric. For. Meteorol.*, *158*, 80–89.

Bleby, T. M., A. J. Mcelrone, and R. B. Jackson (2010), Water uptake and hydraulic redistribution across large woody root systems to 20 m depth, *Plant, Cell Environ.*, *33*(12), 2132–2148.

Boersma, L., F. Lindstrom, and S. Childs (1991), Model for steady state coupled transport in xylem and phloem, *Agron. J.*, *83*(2), 401–408.

Bohrer, G., H. Mourad, T. A. Laursen, D. Drewry, R. Avissar, D. Poggi, R. Oren, and G. G. Katul (2005), Finite element tree crown hydrodynamics model (FETCH) using porous media flow within branching elements: A new representation of tree hydrodynamics, *Water Resour. Res.*, *41*, W11404, doi:10.1029/2005WR004181.

Bonan, G. B. (2002), *Ecological Climatology: Concepts and Applications*, Cambridge Univ. Press, Cambridge, U. K.

Bonan, G. B., K. W. Oleson, M. Vertenstein, S. Levis, X. Zeng, Y. Dai, R. E. Dickinson, and Z.-L. Yang (2002), The land surface climatology of the community land model coupled to the NCAR community climate model*, *J. Clim.*, *15*(22), 3123–3149.

Bonan, G. B., M. Williams, R. A. Fisher, and K. W. Oleson (2014), Modeling stomatal conductance in the Earth system: Linking leaf water-use efficiency and water transport along the soil-plant-atmosphere continuum, *Geosci. Model Dev.*, *7*(5), 2193–2222, doi:10.5194/gmd-7-2193-2014.

Bovard, B. D., P. S. Curtis, C. S. Vogel, H.-B. Su, and H. P. Schmid (2005), Environmental controls on sap flow in a northern hardwood forest, *Tree Physiol.*, *25*, 31–38.

Brodribb, T. J., and N. M. Holbrook (2004), Stomatal protection against hydraulic failure: A comparison of coexisting ferns and angiosperms, *New Phytol.*, *162*(3), 663–670, doi:10.1111/j.1469-8137.2004.01060.x.

Brooks, S. P., and G. O. Roberts (1998), Assessing convergence of Markov chain Monte Carlo algorithms, *Stat. Comput.*, *8*(4), 319–335.

Buckley, T. N. (2005), The control of stomata by water balance, *New Phytol.*, *168*(2), 275–291, doi:10.1111/j.1469-8137.2005.01543.x.

Burnham, K. P., and D. R. Anderson (2002), *Model Selection and Multimodel Inference: A Practical Information-Theoretic Approach*, 2nd ed., Springer, New York, doi:10.1016/S0022-2496(03)00064-6.

Bush, S. E., D. E. Pataki, K. R. Hultine, A. G. West, J. S. Sperry, and J. R. Ehleringer (2008), Wood anatomy constrains stomatal responses to atmospheric vapor pressure deficit in irrigated, urban trees, *Oecologia*, *156*(1), 13–20, doi:10.1007/s00442-008-0966-5.

Caldwell, M. M., and J. H. Richards (1989), Hydraulic lift: Water efflux from upper roots improves effectiveness of water uptake by deep roots, *Oecologia*, *79*(1), 1–5.

Celia, M. A., E. T. Bouloutas, and R. L. Zarba (1990), A general mass-conservative numerical solution for the unsaturated flow equation, *Water Resour. Res.*, *26*(7), 1483–1496, doi:10.1029/90WR00196.

Chen, L., Z. Zhang, Z. Li, J. Tang, P. Caldwell, and W. Zhang (2011), Biophysical control of whole tree transpiration under an urban environment in Northern China, *J. Hydrol.*, *402*(3), 388–400.

Chuang, Y.-L., R. Oren, A. L. Bertozzi, N. Phillips, and G. G. Katul (2006), The porous media model for the hydraulic system of a conifer tree: Linking sap flux data to transpiration rate, *Ecol. Model.*, *191*(3), 447–468, doi:10.1016/j.ecolmodel.2005.03.027.

Clark, K. L., N. Skowronski, and J. Hom (2010), Invasive insects impact forest carbon dynamics, *Global Change Biol.*, *16*(1), 88–101, doi:10.1111/j.1365-2486.2009.01983.x.

Clark, K. L., N. Skowronski, M. Gallagher, H. Renninger, and K. Schaefer (2012), Effects of invasive insects and fire on forest energy exchange and evapotranspiration in the New Jersey pinelands, *Agric. For. Meteorol.*, *166*, 50–61, doi:10.1016/j.agrformet.2012.07.007.

Cowan, I. (1972), An electrical analogue of evaporation from, and flow of water in plants, *Planta*, *106*(3), 221–226, doi:10.1007/BF00388099.

Cowan, I. R., and G. D. Farquhar (1977), Stomatal function in relation to leaf metabolism and environment, in *Society for Experimental Biology Symposium, Integration of Activity in the Higher Plant*, vol. 31, edited by D. H. Jennings, pp. 471–505, Society for Experimental Biology, Cambridge, U. K.

Cruiziat, P., H. Cochard, and T. Améglio (2002), Hydraulic architecture of trees: Main concepts and results, *Ann. For. Sci.*, *59*(7), 723–752, doi:10.1051/forest:2002060.

Davis, S. D., F. W. Ewers, J. S. Sperry, K. A. Portwood, M. C. Crocker, and G. C. Adams (2002), Shoot dieback during prolonged drought in Ceanothus (Rhamnaceae) chaparral of California: A possible case of hydraulic failure, *Am. J. Bot.*, *89*(5), 820–828, doi:10.3732/ajb.89.5.820.

Dighton, J., A. R. Tuininga, D. M. Gray, R. E. Huskins, and T. Belton (2004), Impacts of atmospheric deposition on New Jersey pine barrens forest soils and communities of ectomycorrhizae, *For. Ecol. Manage.*, *201*(1), 131–144, doi:10.1016/j.foreco.2004.07.038.

Domec, J. C., and B. L. Gartner (2003), Relationship between growth rates and xylem hydraulic characteristics in young, mature and old-growth ponderosa pine trees, *Plant, Cell Environ.*, *26*(3), 471–483, doi:10.1046/j.1365-3040.2003.00978.x.

Domec, J.-C., J. Warren, F. Meinzer, J. Brooks, and R. Coulombe (2004), Native root xylem embolism and stomatal closure in stands of Douglas-fir and ponderosa pine: Mitigation by hydraulic redistribution, *Oecologia*, *141*(1), 7–16.

Doussan, C., A. Pierret, E. Garrigues, and L. Pagès (2006), Water uptake by plant roots: II—Modelling of water transfer in the soil root-system with explicit account of flow within the root system—Comparison with experiments, *Plant Soil*, *283*(1–2), 99–117.

Ershadi, A., M. McCabe, J. Evans, N. Chaney, and E. Wood (2014), Multi-site evaluation of terrestrial evaporation models using FLUXNET data, *Agric. For. Meteorol.*, *187*, 46–61, doi:10.1016/j.agrformet.2013.11.008.

Ewers, B. E., and R. Oren (2000), Analyses of assumptions and errors in the calculation of stomatal conductance from sap flux measurements, *Tree Physiol.*, *20*(9), 579–589.

Ewers, B. E., D. S. Mackay, and S. Samanta (2007a), Interannual consistency in canopy stomatal conductance control of leaf water potential across seven tree species, *Tree Physiol.*, *27*(1), 11–24.

Ewers, B. E., R. Oren, H. S. Kim, G. Bohrer, and C. T. Lai (2007b), Effects of hydraulic architecture and spatial variation in light on mean stomatal conductance of tree branches and crowns, *Plant, Cell Environ.*, *30*(4), 483–496.

Farquhar, G., S. V. von Caemmerer, and J. Berry (1980), A biochemical model of photosynthetic CO_2 assimilation in leaves of C_3 species, *Planta*, *149*(1), 78–90, doi:10.1007/BF00386231.

Fatichi, S. (2014), A mechanistic model of stomatal conductance and plant vascular transport International Conference on Computational Methods in Water Resources, Stuttgart, Germany.

Fatichi, S., V. Y. Ivanov, and E. Caporali (2012), A mechanistic ecohydrological model to investigate complex interactions in cold and warm water-controlled environments: 1. Theoretical framework and plot-scale analysis, *J. Adv. Model. Earth Syst.*, *4*, M05002, doi:10.1029/2011ms000086.

Fatichi, S., C. Pappas, and V. Y. Ivanov (2016), Modeling plant–water interactions: An ecohydrological overview from the cell to the global scale, *Wiley Interdiscip. Rev.: Water*, *3*, 327–368, doi:10.1002/wat2.1125.

Feddes, R. A., P. Kowalik, K. Kolinska-Malinka, and H. Zaradny (1976), Simulation of field water uptake by plants using a soil water dependent root extraction function, *J. Hydrol.*, *31*(1), 13–26, doi:10.1016/0022-1694(76)90017-2.

Feddes, R. A., P. J. Kowalik, and H. Zaradny (1978), *Simulation of Field Water Use and Crop Yield*, Pudoc for the Centre for Agricultural Publishing and Documentation, Wageningen.

Feddes, R. A., H. Hoff, M. Bruen, T. Dawson, P. de Rosnay, P. Dirmeyer, R. B. Jackson, P. Kabat, A. Kleidon, and A. Lilly (2001), Modeling root water uptake in hydrological and climate models, *Bull. Am. Meteorol. Soc.*, *82*(12), 2797–2809, doi:10.1175/1520-0477(2001)082<2797:MRWUIH>2.3.CO;2.

Franks, P. J., P. L. Drake, and R. H. Froend (2007), Anisohydric but isohydrodynamic: Seasonally constant plant water potential gradient explained by a stomatal control mechanism incorporating variable plant hydraulic conductance, *Plant, Cell Environ.*, *30*(1), 19–30, doi:10.1111/j.1365-3040.2006.01600.x.

Früh, T., and W. Kurth (1999), The hydraulic system of trees: Theoretical framework and numerical simulation, *J. Theor. Biol.*, *201*(4), 251–270.

Garrity, S. R., K. Meyer, K. D. Maurer, B. Hardiman, and G. Bohrer (2012), Estimating plot-level tree structure in a deciduous forest by combining allometric equations, spatial wavelet analysis and airborne LiDAR, *Remote Sens. Lett.*, *3*(5), 443–451, doi:10.1080/01431161.2011.618814.

Gentine, P., M. Guérin, M. Uriarte, N. G. McDowell, and W. T. Pockman (2015), An allometry-based model of the survival strategies of hydraulic failure and carbon starvation, *Ecohydrology*, doi:10.1002/eco.1654.

Gleason, S. M., et al. (2016), Weak tradeoff between xylem safety and xylem-specific hydraulic efficiency across the world's woody plant species, *New Phytol.*, *209*(1), 123–136, doi:10.1111/nph.13646.

Güneralp, B., and G. Gertner (2007), Feedback loop dominance analysis of two tree mortality models: Relationship between structure and behavior, *Tree Physiol.*, *27*(2), 269–280, doi:10.1093/treephys/27.2.269.

Haario, H., E. Saksman, and J. Tamminen (2001), An adaptive Metropolis algorithm, *Bernoulli*, *7*(2), 223–242.

Haario, H., M. Laine, A. Mira, and E. Saksman (2006), DRAM: Efficient adaptive MCMC, *Stat. Comput.*, *16*(4), 339–354, doi:10.1007/s11222-006-9438-0.

Hacke, U. G., J. S. Sperry, W. T. Pockman, S. D. Davis, and K. A. McCulloh (2001), Trends in wood density and structure are linked to prevention of xylem implosion by negative pressure, *Oecologia*, *126*(4), 457–461, doi:10.1007/s004420100628.

Hardiman, B. S., G. Bohrer, C. M. Gough, C. S. Vogel, and P. S. Curtis (2011), The role of canopy structural complexity in wood net primary production of a maturing northern deciduous forest, *Ecology*, *92*(9), 1818–1827.

Ivanov, V. Y., L. R. Hutyra, S. C. Wofsy, J. W. Munger, S. R. Saleska, R. C. Oliveira, and P. B. Camargo (2012), Root niche separation can explain avoidance of seasonal drought stress and vulnerability of overstory trees to extended drought in a mature Amazonian forest, *Water Resour. Res.*, *48*, W12507, doi:10.1029/2012WR011972.

Janott, M., S. Gayler, A. Gessler, M. Javaux, C. Klier, and E. Priesack (2011), A one-dimensional model of water flow in soil-plant systems based on plant architecture, *Plant Soil*, *341*(1–2), 233–256, doi:10.1007/s11104-010-0639-0.

Jarvis, P. (1976), The interpretation of the variations in leaf water potential and stomatal conductance found in canopies in the field, *Philos. Trans. R. Soc., B*, *273*(927), 593–610, doi:10.1098/rstb.1976.0035.

Katul, G., R. Leuning, and R. Oren (2003), Relationship between plant hydraulic and biochemical properties derived from a steady-state coupled water and carbon transport model, *Plant, Cell Environ.*, *26*(3), 339–350, doi:10.1046/j.1365-3040.2003.00965.x.

Katul, G. G., L. Mahrt, D. Poggi, and C. Sanz (2004), One-and two-equation models for canopy turbulence, *Boundary Layer Meteorol.*, *113*(1), 81–109, doi:10.1023/B:BOUN.0000037333.48760.e5.

Kolb, T., and L. McCormick (1993), Etiology of sugar maple decline in four Pennsylvania stands, *Can. J. For. Res.*, *23*(11), 2395–2402, doi:10.1139/x93-296.

Kumagai, T. O. (2001), Modeling water transportation and storage in sapwood—Model development and validation, *Agric. For. Meteorol.*, *109*(2), 105–115.

Lee, T. J. (1992), *The Impact of Vegetation on the Atmospheric Boundary Layer and Convective Storms*, Colorado State Univ., Fort Collins, Colo.

Lens, F., J. S. Sperry, M. A. Christman, B. Choat, D. Rabaey, and S. Jansen (2011), Testing hypotheses that link wood anatomy to cavitation resistance and hydraulic conductivity in the genus Acer, *New Phytol.*, *190*(3), 709–723, doi:10.1111/j.1469-8137.2010.03518.x.

Mackay, D. S., D. E. Roberts, B. E. Ewers, J. S. Sperry, N. G. McDowell, and W. T. Pockman (2015), Interdependence of chronic hydraulic dysfunction and canopy processes can improve integrated models of tree response to drought, *Water Resour. Res.*, *51*, 6156–6176, doi:10.1002/2015WR017244.

Maherali, H., W. T. Pockman, and R. B. Jackson (2004), Adaptive variation in the vulnerability of woody plants to xylem cavitation, *Ecology*, *85*(8), 2184–2199, doi:10.1890/02-0538.

Maherali, H., C. F. Moura, M. C. Caldeira, C. J. Willson, and R. B. Jackson (2006), Functional coordination between leaf gas exchange and vulnerability to xylem cavitation in temperate forest trees, *Plant, Cell Environ.*, *29*(4), 571–583, doi:10.1111/j.1365-3040.2005.01433.x.

Manzoni, S., G. Vico, G. Katul, S. Palmroth, R. B. Jackson, and A. Porporato (2013), Hydraulic limits on maximum plant transpiration and the emergence of the safety–efficiency trade-off, *New Phytol.*, *198*(1), 169–178, doi:10.1111/nph.12126.

Matheny, A. M., et al. (2014a), Characterizing the diurnal patterns of errors in the prediction of evapotranspiration by several land-surface models: An NACP analysis, *Biogeosciences*, *119*(7), 1458–1473, doi:10.1002/2014JG002623.

Matheny, A. M., et al. (2014b), Species-specific transpiration responses to intermediate disturbance in a northern hardwood forest, *J. Geophys. Res. Biogeosci.*, *119*, 2292–2311, doi:10.1002/2014JG002623.

Matheny, A. M., G. Bohrer, S. R. Garrity, C. J. Howard, and C. S. Vogel (2015), Observations of stem water storage in trees of opposing hydraulic strategies, *Ecosphere*, doi:10.1890/ES15-00170.1.

Mayr, S., F. Schwienbacher, and H. Bauer (2003), Winter at the alpine timberline. Why does embolism occur in Norway spruce but not in stone pine?, *Plant Physiol.*, *131*(2), 780–792, doi:10.1104/pp.011452.

McAdam, S. A., and T. J. Brodribb (2014), Separating Active and Passive Influences on Stomatal Control of Transpiration [OPEN], *Plant Physiol.*, *164*(4), 1578–1586, doi:10.1104/pp.113.231944.

McCulloh, K. A., and J. S. Sperry (2005), Patterns in hydraulic architecture and implications for transport efficiency, *Tree Physiol.*, *25*, 257–267, doi:10.1093/treephys/25.3.257.

McCulloh, K. A., D. M. Johnson, F. C. Meinzer, S. L. Voelker, B. Lachenbruch, and J.-C. Domec (2012), Hydraulic architecture of two species differing in wood density: Opposing strategies in co-occurring tropical pioneer trees, *Plant, Cell Environ.*, *35*(1), 116–125, doi:10.1111/j.1365-3040.2011.02421.x.

McDowell, N. G., et al. (2013), Evaluating theories of drought-induced vegetation mortality using a multimodel-experiment framework, *New Phytol.*, *200*(2), 304–321, doi:10.1111/nph.12465.

McDowell, N., W. T. Pockman, C. D. Allen, D. D. Breshears, N. Cobb, T. Kolb, J. Plaut, J. Sperry, A. West, and D. G. Williams (2008), Mechanisms of plant survival and mortality during drought: Why do some plants survive while others succumb to drought?, *New Phytol.*, *178*(4), 719–739, doi:10.1111/j.1469-8137.2008.02436.x.

Medlyn, B. E., A. P. Robinson, R. Clement, and R. E. McMurtrie (2005), On the validation of models of forest CO_2 exchange using eddy covariance data: Some perils and pitfalls, *Tree Physiol.*, *25*(7), 839–857, doi:10.1093/treephys/25.7.839.

Medvigy, D., S. C. Wofsy, J. W. Munger, D. Y. Hollinger, and P. R. Moorcroft (2009), Mechanistic scaling of ecosystem function and dynamics in space and time: Ecosystem Demography model version 2, *J. Geophys. Res.*, *114*, G01002, doi:10.1029/2008JG000812.

Meinzer, F., S. James, G. Goldstein, and D. Woodruff (2003), Whole-tree water transport scales with sapwood capacitance in tropical forest canopy trees, *Plant, Cell Environ.*, *26*(7), 1147–1155, doi:10.1046/j.1365-3040.2003.01039.x.

Meinzer, F. C., and K. A. McCulloh (2013), Xylem recovery from drought-induced embolism: Where is the hydraulic point of no return?, *Tree Physiol.*, *33*(4), 331–334, doi:10.1093/treephys/tpt022.

Meinzer, F. C., K. A. McCulloh, B. Lachenbruch, D. R. Woodruff, and D. M. Johnson (2010), The blind men and the elephant: The impact of context and scale in evaluating conflicts between plant hydraulic safety and efficiency, *Oecologia*, *164*(2), 287–296, doi:10.1007/s00442-010-1734-x.

Meinzer, F. C., D. R. Woodruff, D. M. Eissenstat, H. S. Lin, T. S. Adams, and K. A. McCulloh (2013), Above-and belowground controls on water use by trees of different wood types in an eastern US deciduous forest, *Tree Physiol.*, *33*(4), 345–356, doi:10.1093/treephys/tpt012.

Meinzer, F. C., D. R. Woodruff, D. E. Marias, K. A. McCulloh, and S. Sevanto (2014), Dynamics of leaf water relations components in co-occurring iso-and anisohydric conifer species, *Plant, Cell Environ.*, *37*(11), 2577–2586, doi:10.1111/pce.12327.

Monteith, J. (1965), Evaporation and environment, paper presented at Symp. Soc. Exp. Biol.

Monteith, J. L. (1995), A reinterpretation of stomatal responses to humidity, *Plant, Cell Environ.*, *18*(4), 357–364, doi:10.1111/j.1365-3040.1995.tb00371.x.

Morin, T., G. Bohrer, L. Naor-Azrieli, S. Mesi, W. Kenny, W. Mitsch, and K. Schäfer (2014), The seasonal and diurnal dynamics of methane flux at a created urban wetland, *Ecol. Eng.*, doi:10.1016/j.ecoleng.2014.02.002.

Nikinmaa, E., R. Sievanen, and T. Holtta (2014), Dynamics of leaf gas exchange, xylem and phloem transport, water potential and carbohydrate concentration in a realistic 3-D model tree crown, *Ann. Bot.*, *114*(4), 653–666, doi:10.1093/aob/mcu068.

Novick, K., S. Brantley, C. F. Miniat, J. Walker, and J. M. Vose (2014), Inferring the contribution of advection to total ecosystem scalar fluxes over a tall forest in complex terrain, *Agric. For. Meteorol.*, *185*, 1–13, doi:10.1016/j.agrformet.2013.10.010.

O'Brien, J. J., S. F. Oberbauer, and D. B. Clark (2004), Whole tree xylem sap flow responses to multiple environmental variables in a wet tropical forest, *Plant, Cell Environ.*, *27*(5), 551–567, doi:10.1111/j.1365-3040.2003.01160.x.

Ogle, K., T. G. Whitham, and N. S. Cobb (2000), Tree-ring variation in pinyon predicts likelihood of death following severe drought, *Ecology*, *81*(11), 3237–3243, doi:10.1890/0012-9658(2000)081[3237:TRVIPP]2.0.CO;2.

O'Grady, A. P., D. Worledge, and M. Battaglia (2008), Constraints on transpiration of *Eucalyptus globulus* in southern Tasmania, Australia, *Agric. For. Meteorol.*, *148*(3), 453–465, doi:10.1016/j.agrformet.2007.10.006.

Pan, Y., R. Birdsey, J. Hom, K. McCullough, and K. Clark (2006), Improved estimates of net primary productivity from MODIS satellite data at regional and local scales, *Ecol. Appl.*, *16*(1), 125–132, doi:10.1890/05-0247.

Papale, D., M. Reichstein, M. Aubinet, E. Canfora, C. Bernhofer, W. Kutsch, B. Longdoz, S. Rambal, R. Valentini, and T. Vesala (2006), Towards a standardized processing of net ecosystem exchange measured with eddy covariance technique: Algorithms and uncertainty estimation, *Biogeosciences*, *3*(4), 571–583.

Pappas, C., S. Fatichi, and P. Burlando (2016), Modeling terrestrial carbon and water dynamics across climatic gradients: Does plant trait diversity matter?, *New Phytol.*, *209*(1), 137–151, doi:10.1111/nph.13590.

Penman, H. L. (1948), Natural evaporation from open water, bare soil and grass, paper presented at Proceedings of the Royal Society of London A: Mathematical, Physical and Engineering Sciences, The Royal Society.

Phillips, N., M. Ryan, B. Bond, N. McDowell, T. Hinckley, and J. Čermák (2003), Reliance on stored water increases with tree size in three species in the Pacific Northwest, *Tree Physiol.*, *23*(4), 237–245, doi:10.1093/treephys/23.4.237.

Pittermann, J., J. S. Sperry, U. G. Hacke, J. K. Wheeler, and E. H. Sikkema (2005), Torus-margo pits help conifers compete with angiosperms, *Science*, *310*(5756), 1924–1924, doi:10.1126/science.1120479.

Poggi, D., A. Porporato, L. Ridolfi, J. Albertson, and G. Katul (2004), The effect of vegetation density on canopy sub-layer turbulence, *Boundary Layer Meteorol.*, *111*(3), 565–587, doi:10.1023/B:BOUN.0000016576.05621.73.

Renninger, H. J., and K. V. Schäfer (2012), Comparison of tissue heat balance-and thermal dissipation-derived sap flow measurements in ring-porous oaks and a pine, *Front. Plant Sci.*, *3*, 103, doi:10.3389/fpls.2012.00103.

Renninger, H. J., K. L. Clark, N. Skowronski, and K. V. Schäfer (2013), Effects of a prescribed fire on water use and photosynthetic capacity of pitch pines, *Trees*, *27*(4), 1115–1127, doi:10.1007/s00468-013-0861-5.

Renninger, H. J., N. Carlo, K. L. Clark, and K. V. Schäfer (2014), Physiological strategies of co-occurring oaks in a water-and nutrient-limited ecosystem, *Tree Physiol.*, *34*(2), 159–173, doi:10.1093/treephys/tpt122.

Renninger, H. J., N. J. Carlo, K. L. Clark, and K. V. R. Schaefer (2015), Resource use and efficiency, and stomatal responses to environmental drivers of oak and pine species in an Atlantic Coastal Plain forest, *Front. Plant Sci.*, *6*, 297, doi:10.3389/fpls.2015.00297.

Robinson, J. L., L. D. Slater, and K. V. R. Schaefer (2012), Evidence for spatial variability in hydraulic redistribution within an oak-pine forest from resistivity imaging, *J. Hydrol.*, *430*, 69–79, doi:10.1016/j.jhydrol.2012.02.002.

Roman, D., K. Novick, E. Brzostek, D. Dragoni, F. Rahman, and R. Phillips (2015), The role of isohydric and anisohydric species in determining ecosystem-scale response to severe drought, *Oecologia*, *179*(3), 641–654, doi:10.1007/s00442-015-3380-9.

Sack, L., and N. M. Holbrook (2006), Leaf hydraulics, in *Annual Review of Plant Biology*, edited by S. S. Merchant, pp. 361–381, Annual Reviews, Palo Alto, doi:10.1146/annurev.arplant.56.032604.144141.

Schäfer, K. V. R., K. L. Clark, N. Skowronski, and E. P. Hamerlynck (2010), Impact of insect defoliation on forest carbon balance as assessed with a canopy assimilation model, *Global Change Biol.*, *16*(2), 546–560, doi:10.1111/j.1365-2486.2009.02037.x.

Schäfer, K., H. Renninger, K. Clark, and D. Medvigy (2014), Hydrological responses to defoliation and drought of an upland oak/pine forest, *Hydrol. Processes*, *28*(25), 6113–6123, doi:10.1002/hyp.10104.

Sheriff, D. (1973), Significance of the occurrence of time lags in the transmission of hydraulic shock waves through plant stems, *J. Exp. Bot.*, *24*(5), 796–803, doi:10.1093/jxb/24.5.796.

Siau, J. (1983), A proposed theory for nonisothermal unsteady-state transport of moisture in wood, *Wood Sci. Technol.*, *17*(1), 75–77, doi:10.1007/BF00351834.

Siqueira, M., G. Katul, and A. Porporato (2008), Onset of water stress, hysteresis in plant conductance, and hydraulic lift: Scaling soil water dynamics from millimeters to meters, *Water Resour. Res.*, *44*, W01432, doi:10.1029/2007WR006094.

Sivandran, G., and R. L. Bras (2013), Dynamic root distributions in ecohydrological modeling: A case study at Walnut Gulch Experimental Watershed, *Water Resour. Res.*, *49*, 3292–3305, doi:10.1002/wrcr.20245.

Sperry, J., N. Alder, and S. Eastlack (1993), The effect of reduced hydraulic conductance on stomatal conductance and xylem cavitation, *J. Exp. Bot.*, *44*(6), 1075–1082, doi:10.1093/jxb/44.6.1075.

Sperry, J., F. Adler, G. Campbell, and J. Comstock (1998), Limitation of plant water use by rhizosphere and xylem conductance: Results from a model, *Plant, Cell Environ.*, *21*(4), 347–359, doi:10.1046/j.1365-3040.1998.00287.x.

Sperry, J. S. (2000), Hydraulic constraints on plant gas exchange, *Agric. For. Meteorol.*, *104*(1), 13–23, doi:10.1016/S0168-1923(00)00144-1.

Sperry, J. S. (2003), Evolution of water transport and xylem structure, *Int. J. Plant Sci.*, *164*(S3), S115–S127, doi:10.1086/368398.

Sperry, J. S., U. G. Hacke, R. Oren, and J. P. Comstock (2002), Water deficits and hydraulic limits to leaf water supply, *Plant, Cell Environ.*, *25*(2), 251–263, doi:10.1046/j.0016-8025.2001.00799.x.

Sperry, J. S., V. Stiller, and U. G. Hacke (2003), Xylem hydraulics and the soil–plant–atmosphere continuum, *Agron. J.*, *95*(6), 1362–1370, doi:10.2134/agronj2003.1362.

Stannard, D. I. (1993), Comparison of Penman-Monteith, Shuttleworth-Wallace, and modified Priestley-Taylor evapotranspiration models for wildland vegetation in semiarid rangeland, *Water Resour. Res.*, *29*(5), 1379–1392, doi:10.1029/93WR00333.

Steppe, K., and R. Lemeur (2007), Effects of ring-porous and diffuse-porous stem wood anatomy on the hydraulic parameters used in a water flow and storage model, *Tree Physiol.*, *27*(1), 43–52, doi:10.1093/treephys/27.1.43.

Steppe, K., D. J. W. De Pauw, R. Lemeur, and P. A. Vanrolleghem (2006), A mathematical model linking tree sap flow dynamics to daily stem diameter fluctuations and radial stem growth, *Tree Physiol.*, *26*(3), 257–273, doi:10.1093/treephys/26.3.257.

Taneda, H., and J. S. Sperry (2008), A case-study of water transport in co-occurring ring-versus diffuse-porous trees: Contrasts in water-status, conducting capacity, cavitation and vessel refilling, *Tree Physiol.*, *28*(11), 1641–1651, doi:10.1093/treephys/28.11.1641.

Tardieu, F., and W. J. Davies (1993), Integration of hydraulic and chemical signalling in the control of stomatal conductance and water status of droughted plants, *Plant, Cell Environ.*, *16*(4), 341–349, doi:10.1111/j.1365-3040.1993.tb00880.x.

Tardieu, F., and T. Simonneau (1998), Variability among species of stomatal control under fluctuating soil water status and evaporative demand: Modelling isohydric and anisohydric behaviours, *J. Exp. Bot.*, *49*(Special Issue), 419–432, doi:10.1093/jxb/49.Special_Issue.419.

Taylor, J. R. (1982), *An Introduction to Error Analysis: The Study of Uncertainties in Physical Measurements*, 327 pp., Univ. Sci. Books, Mill Valley, Calif.

Thom, A. (1972), Momentum, mass and heat exchange of vegetation, *Q. J. R. Meteorol. Soc.*, *98*(415), 124–134, doi:10.1002/qj.49709841510.

Thomsen, J., G. Bohrer, A. Matheny, V. Y. Ivanov, L. He, H. Renninger, and K. Schäfer (2013), Contrasting hydraulic strategies during dry soil conditions in *Quercus rubra* and *Acer rubrum* in a sandy site in Michigan, *Forests*, *4*(4), 1106–1120, doi:10.3390/f4041106.

Turner, N. C., E.-D. Schulze, and T. Gollan (1984), The responses of stomata and leaf gas exchange to vapour pressure deficits and soil water content, *Oecologia*, *63*(3), 338–342, doi:10.1007/BF00390662.

Tyree, M. T., and M. H. Zimmermann (2002), Xylem structure and the ascent of sap, in *Xylem Structure and the Ascent of Sap*, 2nd ed., edited by T. E. Timell, pp. 1–283, Springer, Berlin.

Tyree, M. T., S. D. Davis, and H. Cochard (1994), Biophysical perspectives of xylem evolution: Is there a tradeoff of hydraulic efficiency for vulnerability to dysfunction?, *Int. Assoc. Wood Anat. J.*, *15*(4), 335–360, doi:10.1163/22941932-90001369.

Unsworth, M. H., N. Phillips, T. Link, B. J. Bond, M. Falk, M. E. Harmon, T. M. Hinckley, D. Marks, and K. T. Paw U (2004), Components and controls of water flux in an old-growth Douglas-fir-western hemlock ecosystem, *Ecosystems*, *7*(5), 468–481, doi:10.1007/s10021-004-0138-3.

Van den Honert, T. (1948), Water transport in plants as a catenary process, *Discuss. Faraday Soc.*, *3*, 146–153, doi:10.1039/df9480300146.

Verbeeck, H., K. Steppe, N. Nadezhdina, M. O. De Beeck, G. Deckmyn, L. Meiresonne, R. Lemeur, R. Ceulemans, and I. Janssens (2007a), Model analysis of the effects of atmospheric drivers on storage water use in Scots pine, *Biogeosciences*, *4*(4), 657–671.

Verbeeck, H., K. Steppe, N. Nadezhdina, M. Op de Beeck, G. Deckmyn, L. Meiresonne, R. Lemeur, J. Cermak, R. Ceulemans, and I. A. Janssens (2007b), Stored water use and transpiration in Scots pine: A modeling analysis with ANAFORE, *Tree Physiol.*, *27*(12), 1671–1685, doi:10.1093/treephys/27.12.1671.

Verma, P., S. P. Loheide II, D. Eamus, and E. Daly (2014), Root water compensation sustains transpiration rates in an Australian woodland, *Adv. Water Resour.*, *74*, 91–101, doi:10.1016/j.advwatres.2014.08.013.

Vrugt, J., J. Hopmans, and J. Šimunek (2001), Calibration of a two-dimensional root water uptake model, *Soil Sci. Soc. Am. J.*, *65*(4), 1027–1037.

Whitehead, D. (1998), Regulation of stomatal conductance and transpiration in forest canopies, *Tree Physiol.*, *18*(8–9), 633–644, doi:10.1093/treephys/18.8-9.633.

Williams, D., W. Cable, K. Hultine, J. Hoedjes, E. Yepez, V. Simonneaux, S. Er-Raki, G. Boulet, H. De Bruin, and A. Chehbouni (2004), Evapotranspiration components determined by stable isotope, sap flow and eddy covariance techniques, *Agric. For. Meteorol.*, *125*(3), 241–258, doi:10.1016/j.agrformet.2004.04.008.

Zhang, Q., S. Manzoni, G. G. Katul, A. Porporato, and D. Yang (2014), The hysteretic evapotranspiration—Vapor pressure deficit relation, *J. Geophys. Res. Biogeosci.*, *19*, 125–140, doi:10.1002/2013JG002484.